Exploring the potential of MXene-based advanced solar-absorber in improving the performance and efficiency of a solar-desalination unit for brackish water purification

Amrit Kumar Thakur[1*], Ravishankar Sathyamurthy[1*], R. Saidur[2,3*], R. Velraj[4], I. Lynch[5*], Navid Aslfattahi[6]

[1] Department of Mechanical Engineering, KPR Institute of Engineering and Technology, Arasur, Coimbatore, Tamil Nadu, 641407, India

[2] Research Center for Nano-Materials and Energy Technology (RCNMET), School of Engineering and Technology, Sunway University, Bandar Sunway, Petaling Jaya, 47500, Selangor Darul Ehsan, Malaysia

[3]Department of Engineering, Lancaster University, Lancaster, LA1 4YW, UK

[4] Institute for Energy Studies, Anna University, Chennai, 600025, Tamilnadu, India

[5] School of Geography, Earth and Environmental Sciences, University of Birmingham, Edgbaston, B15 2TT Birmingham, UK

[6] Department of Mechanical Engineering, Faculty of Engineering, University of Malaya, 50603, Kuala Lumpur, Malaysia

***Corresponding authors**

Amrit Kumar Thakur (amritt1@gmail.com)

Ravishankar Sathyamurthy (raviannauniv23@gmail.com)

R. Saidur (saidur@sunway.edu.my)

I. Lynch (I.Lynch@bham.ac.uk)

Abstract

Brackish water desalination using solar still (SS) is a low-cost sustainable solution to global water scarcity, but this technology suffers from low yield and efficiency. The judicious amalgamation of highly conductive materials with superior solar absorption behavior is one of the most effective approaches to overcome this limitation. In this regard, the present work synthesizes a novel multilayered 2-D MXene from 3-D MAX phase as a coating material for the solar absorber of a SS to improve its performance. Two different loadings of MXene (0.05 and 0.1 wt. %) were dispersed in turpentine oil/black paint (1:4) and coated onto the solar absorber of the SS. Higher MXene loading significantly augmented the thermal conductivity and solar absorptivity of the turpentine oil/black paint solution. The 0.1 wt. % MXene coated absorber provided a higher heat transfer rate from the absorber to the water, leading to a 6 % increase in water temperature and a total water yield of 2.07 kg. The theoretical calculated water yield was identical to the experimental yield with a deviation of ± 5 %, demonstrating the accuracy of thermal modelling. The average energy efficiency of the SS with 0.1 wt. % MXene in the absorber black paint coating was 36.31 %. Water quality analysis shown that the distilled water resulting from the desalination is suitable for drinking. In conclusion, MXene with its excellent thermo-physical properties and solar absorptivity will be beneficial in development of efficient solar desalination units with augmented performance for water purification.

Keywords: MXene, Solar Desalination, Thermal performance, Absorber coating, Water quality, Energy efficiency

I. Introduction

Ecosystems, life and sustainable growth all depend fully on the availability of fresh water sources. Circulating waters, which are the sources of clean water on this planet, are progressively shrinking

in volume. On earth, 96.54 % of the water is sea-water and of the 2.53 % that is freshwater, just 0.36 % is accessible, with the rest tied up in glaciers and the polar icecaps. With increasing global population and urbanization, water demand has tremendously increased over the last decades, leading to severe exploitation of available water resources. Freshwater insufficiency is the foremost threat for humans [1-3]. Thus, it is very important to explore effective methods for generating clean water from other sources such as seawater, wastewater, and contaminated ground water [4].

Sea-water desalination is the most promising method to meet the escalating worldwide requirements for freshwater. Large scale commercial desalination units, operated by mechanical or thermal energy, are already available and in operation, utilizing technologies such as membrane distillation, humidification-dehumidification, reverse osmosis, and multistage distillation units [5-7]. However, these desalination methods necessitate centralized units along with developed infrastructure, and thus, they are not suitable for rural and remote places with severe clean water scarcity [8]. Small sized compact passive desalting units with low maintenance costs could be easily deployed in such locations to fulfill the freshwater demands and improve local living standards. Solar still (SS) is the simplest and most reliable passive type desalination unit which convert sun-light into thermal energy used to purify brackish water through distillation making it potable [9]. Conventional SS mainly rely on the ‘solar absorption’ and heating a bulk brackish water to promote vaporization, which is then utilized to collect the purified water through condensation. However, the major limitation of conventional SS is its low ‘solar thermal’ cumulative efficiency (defined as the total evaporation enthalpy of the distillate water over the total energy from the sun-light input), as the large quantity of cold bulk brackish water used as

input requires a lot of solar energy to be heated (distilled). The thermal and optical losses of these systems also significantly contribute towards their low efficiency.

To increase the water yield and efficiency of the SS, various studies have been performed using different enhancement approaches, including design modifications in the structure by designing a wick type SS [10], stepped SS [11], double slope SS [12] etc. Utilization of highly porous materials for enhancing water and glass cover temperature difference [13-14], carbon based materials for improved solar absorption [15] and phase change materials [16] for prolonged heat supply in the still basin have been widely used for augmented water yield in recent years. At present, the water yield of a conventional SS is generally 2-5 kg/m^2 [17] with an energy efficiency of 30 - 50 % [18] and thus, there is still ample work required to further improve its performance. With significant development in materials science and nanotechnology, various researches have explored the role of coating the SS absorber using nanoparticles for increasing the solar absorption and augmenting the water yield. Arunkumar et al. [19] explored ZnO, CuO, MoO_3 as coating materials for the solar absorber and examined their effects on the water yield of the SS. It was found that the CuO coated SS exhibited the highest water yield amongst all coatings tested. Thakur et al. [20] synthesized reduced graphene oxide (RGO) using the Hummer method and coated it by mixing with black paint onto the absorber of the SS. Results revealed that 12 wt. % RGO mixed into the black paint coated solar absorber increased the water yield of the SS by 41.1 %. In similar way, Sathyamurthy et al. [21] used 20 wt. % nano-silicon oxide mixed black paint coating on the absorber which improved the water productivity by 34.2 %. Kabeel et al. [22] utilized 0.1 % titanium dioxide doped into black paint to coat the absorber and enhanced the water yield of SS by 6.1 %. Some other emerging materials are also being developed [23-27]. It is inferred from the above outcomes that doping of conductive nanomaterials with higher solar absorption into black paint to coat the

absorber increases the solar absorption, leading to higher water yield. However, all the reported work used higher loading of nanoparticles, which could leads to thermal performance degradation over the time. In addition, the higher mass fraction of nanoparticles could leads to poor life cycle owing to the lower uniformity in coating while applying onto the absorber. Consequently, the thermal performance of the absorber can be drastically affected if there is lower compatibility between the absorber and paint which could be due to the excessive amount of nanoparticle dispersion in the paint. It is also important to mention that owing to higher loading of nanoparticle which exhibits higher cost of synthesis, the overall cost of the still could significantly increase that may hinders its application in remote and rural locations for fulfillment of fresh water needs. Since, the solar stills are used throughout the year to produce portable water from the seawater / brackish water, the selection of absorber coating should be in the view of long term stability along with excellent solar absorption behavior. Therefore, nanomaterials with high temperature stability, excellent solar-absorption and low emissivity behavior (selective coating) along with higher specific surface area and thermal conductivity with optimum mass fraction should be selected for the absorber coating in order to improve the thermal performance of the SS.

In 2011, Gogotsi's group introduced MXene, 2-D transition metal carbides, nitrides and carbonitrides, which have been widely explored in several applications such as energy storage [28], heat transfer fluid [29], molecular sieves [30], and electromagnetic interference shielding [31] owing to its unique adjustable surface chemistry, high aspect ratio, and excellent electrical and mechanical properties [32-33]. Among the family of MXene materials, particularly Ti_3C_2 exhibited excellent photo-thermal conversion behavior with a conversion efficiency ('light' to 'heat') of 100 %, which can completely absorb and dissipate the electromagnetic radiation as heat [34-36]. With the aforementioned absorption behavior of MXene, it is potentially very beneficial

for solar steam generation and evaporation. Ming et al. [37] developed MXene/GO aerogel for solar based steam generation and demonstrated superior evaporation efficiency of 90.7 % (only 63.7 % for graphene oxide aerogel) and evaporation rate of 1.27 kg/m^{2}h (0.88 kg/m^2 for graphene oxide aerogel), respectively under 1 sun (1 kW/m^2) irradiation. Li et al. [38] demonstrated 100 % internal light-to-heat conversion efficiency of MXene following fabrication of a thin self-floating membrane using exfoliated MXene which exhibited solar based evaporation efficiency of 84%. Li et al. [39] developed a novel MXene nanocoating which exhibited 93.2 % light absorption (broadband) and solar energy conversion efficiency of 90.1 % for steam generation.

Thus, MXene has demonstrated an excellent prospective in improving solar absorption and water evaporation. These encouraging properties together with high thermal conductivity [40] make MXene a most suitable candidate for coating of the solar absorber in the desalination unit under moderate temperature conditions. However, coating of the solar absorber with MXene for increasing the water yield of the desalination unit has not been reported to date. Therefore, to improve the performance of solar desalination unit though absorber coating approach, the present work explored MXene as a potential candidate with a lower mass fraction. In this view, we synthesized a multilayer MXene by *in-situ* etching and explored its role on augmenting the overall performance of the desalination unit under Indian climatic conditions. A detailed in-depth surface morphological analysis of synthesized MXene was carried out using scanning electron microscopy with energy dispersive X-ray spectroscopic along with elemental mapping to analyse the microstructures. Further, powder X-ray diffraction and thermo gravimetric analysis were done to ascertain the chemical purity and thermal stability of the MXene powder. Afterward, MXene was doped into black paint at different mass fractions (0.05 wt. % and 0.1 wt. %) and coated onto the solar absorber to increase the thermal performance and water yield. In addition, detailed

thermodynamic analysis with energy efficiency and water quality analysis were carried out and discussed. The thermal performance and evaporation/condensation investigation provides an optimization arrangement and analysis scheme for solar desalination units containing high absorption and photo-thermal conversion based absorbers generated with novel 2-D materials. We believe that the in-depth analysis of MXene synthesis and its application for generating freshwater will definitely pave the path in development of portable solar desalination unit with excellent overall efficiency and the demonstrated approach could be potentially used to generate clean water in remote and rural location globally with minimal initial investment.

2. Development of MXene based solar absorber

2.1 Synthesis of MXene (Ti_3C_2)

The MXene ($Ti_3C_2T_x$) synthesis procedure was carried out using the following materials as received without any auxiliary purification: MAX Phase (Ti_3AlC_2) material from Y-Carbon Limited, 95 % reagent grade ammonium hydrogen difluoride (Sigma Aldrich, USA) and sodium hydroxide (pellets 97 % purity, Sigma Aldrich, USA). A common synthesis route, the wet-chemistry etching technique, was considered for the production of the MXene nanomaterial. Preparation of 2M solution of NH_4HF_2 as etchant was the initiated step in order to commence the required etching process. The prepared 20 mL ammonium hydrogen difluoride solution was placed on the hot plate magnetic stirrer with stirring for 1 h at 300 rpm and 30 °C. Afterwards, 1 g of Ti_3AlC_2 was weighed using a microbalance, and added to the uniformly well-prepared NH_4HF_2 solution. Addition of Ti_3AlC_2 to the NH_4HF_2 solution was carried out slowly due to the exothermic nature of the reaction. The Ti_3AlC_2 suspension in the NH_4HF_2 was magnetically-stirred for 48 h at 300 rpm and 30 °C for continuous conduction of etching process. Upon completion of etching process, the pH of the solution was controlled using a dilute solution of NaOH in order to reach

pH 6, followed by filtering/rinsing of the product numerous times with deionized water. A washing process was performed using an ultrahigh centrifuge (Sorvall LYNX 6000, Thermo Scientific) four times (each time of 10 minutes) at 3500 rpm. The achieved multi-layered $Ti_3C_2T_x$ solution was then sonicated using an ultrasonic probe sonicator (FS-1200N) for one hour with the settings of power 60 % and on/off time of 7/3 seconds to obtain delaminated MXene (d-$Ti_3C_2T_x$). Afterward, delaminated flakes of synthesized MXene nanomaterial were dried in a vacuum oven (VO 500, MEMMERT Germany) overnight.

2.2 Structural characterization of pure MXene (Ti_3C_2)

Scanning electron microscopy (SEM) was done in a Gemini-300 (Carl ZEISS, Germany), using an accelerating voltage of 10 kV and a working distance of 10 mm, which was used to analyze the morphology and particle size. Energy Dispersive X-ray Spectroscopic (EDX) analysis along with element weight percentages of Ti_3C_2 were analyzed by Oxford Instruments (Oxfordshire, UK). Powder X-ray diffraction (XRD) analysis was carried out using a Smart lab diffractometer (Rigaku, Tokyo, Japan) with Cu Kα radiation (wavelength = 0.15406 nm) working in the reflection mode with 'Bragg-Brentano' geometry for investigation of the crystalline structure. Thermogravimetric analysis (TGA) of the MXene was conducted using SDT-Q600 (TA Instruments, USA) from 30 to 800 °C to analyse the decomposition of the sample and the heating rate was maintained at 10 °C/min.

2.3 Preparation and development of the MXene coated solar absorber

After the synthesis of MXene, the MXene coated solar absorber was developed to augment the performance of the desalination unit. Firstly, extrapure turpentine oil (Sisco Research Laboratories Pvt. Ltd. India) was used to disperse two different mass concentrations of MXene (0.05, and 0.1 wt. %). The solutions were stirred for 30 min using a magnetic stirrer at 1000 rpm to uniformly

mix the MXene into the oil. Afterwards, the solution was subjected to sonication using a probe sonicator (Samarth Electronics, Model no - SM750PS, India) for 30 min at 15 kHz to achieve a homogeneous mixture of MXene/oil and then, their thermal conductivity were measured.

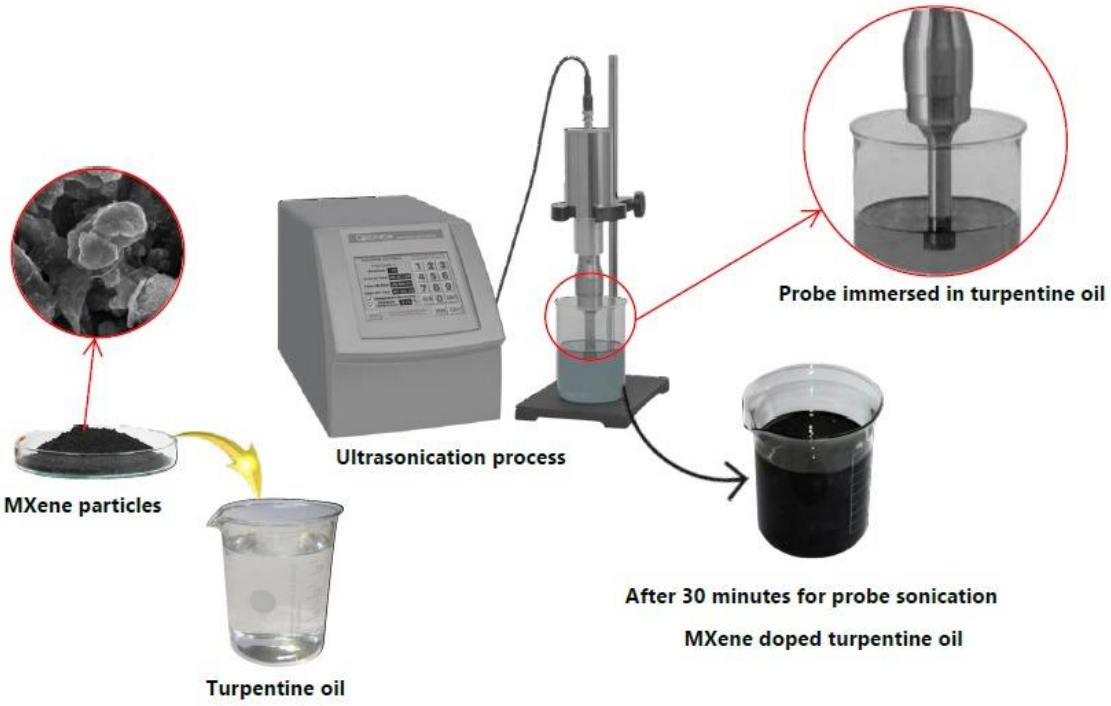

Fig. 1. Steps involved in the preparation of turpentine oil/ MXene solution

Afterward, black chrome paint was mixed into the solution (turpentine: black paint = 1:4) and sonicated for 30 min to achieve a uniform MXene based conductive nano-paint solution. The schematic of MXene-based nanopaint preparation is presented in Fig. 1. The solution was then transferred into the spray gun (Air-ga H827 Hvlp) and the solar absorber of the SS (1.6 mm thick galvanized iron (G.I), absorber area = 0.5 m^2) was coated using the MXene paint with air consumption of 6 cubic feet per minute (CFM). The solar absorbers of the SS were dried in ambient conditions for 120 h and assessed in terms of their improvement of the performance of the desalination unit.

2.4 Thermal and optical properties analysis of MXene based paint

2.4.1 Thermal conductivity measurement

The thermal conductivity (TC) of the coated absorber is very significant in terms of increasing the water evaporation, leading to a higher water yield from the desalination unit and therefore, its accurate measurement is essential. In this regard, the MXene/Turpentine oil solution thermal conductivities were measured using KD2-Pro Thermal analyzer (Decagon Devices, United States of America), and the schematic view of the TC measuring device is presented in Fig. 2.

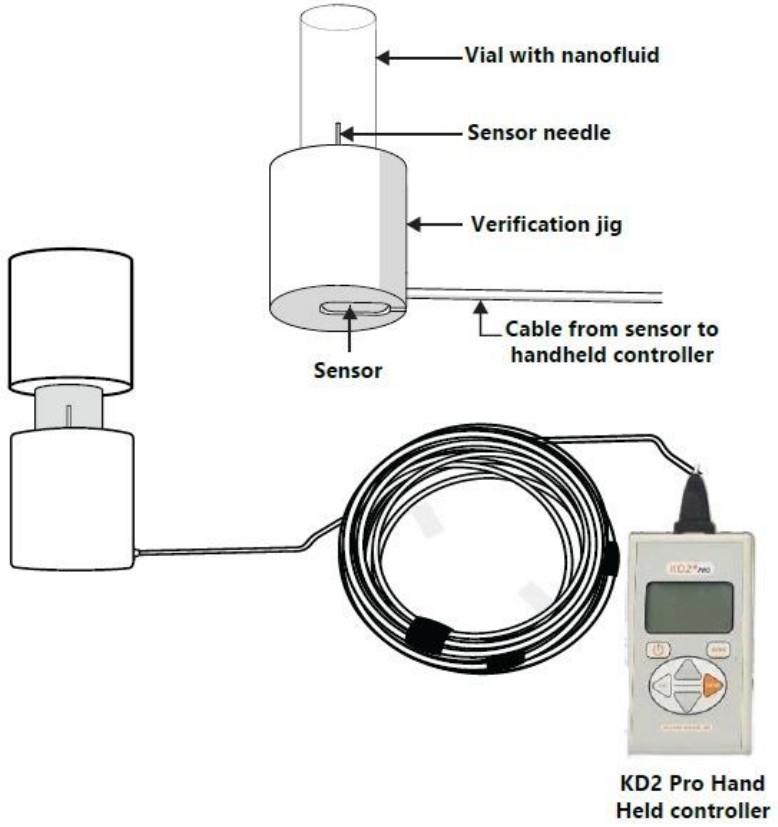

Fig. 2. Schematic of thermal conductivity measurement set up

The thermal conductivity analyser works based on a transient hot-wire method. The TC of the turpentine oil and MXene/Turpentine oil solutions were measured at 30 °C using a probe sensor (1.27 mm diameter, 60 mm length). Initially the MXene/ turpentine oil solution was placed in a glass vial and maintained in a constant temperature water bath (accuracy of ± 0.1 °C) at 30 °C. The

needle was then inserted at the center of the vial and thermal conductivity was measured. For each MXene/Turpentine oil solution, three measurements were carried out to get accurate results.

2.4.2 Ultraviolet-visible (UV-Vis) spectroscopy analysis

In a solar desalination unit, the absorber plays the most important role in enhancing the evaporation rate and it should have high absorption behavior. Thus, it is very important to determine the solar absorption behavior of the powder MXene and MXene based nano-coating. The optical absorbance of the powder MXene and absorber coated with bare black paint and black paint dispersed with two different mass fraction of MXene were investigated using UV-Vis spectrophotometry. The spectra were acquired using a Perkin Elmer LAMBDA 750 for powder sample and Perkin Elmer LAMBDA 950 for painted absorber, respectively. The data were collected at room temperature scanning the wavelengths from 200 nm to 1100 nm.

3. Experimental set-up and data analysis

In the present work, three identical single basin SS were fabricated: (i) Conventional SS with bare black paint coated absorber (CSS), (ii) modified SS with black paint mixed with 0.05 wt. % MXene coated absorber (CSS-0.05 wt. % MXene), and (iii) modified SS with black paint mixed with 0.1 wt. % MXene coated absorber (CSS-0.1 wt. % MXene). These were tested in parallel under the climatic conditions of Chennai, Tamilnadu (13.01° N, 80.24° E), India in the month of May, 2021. Single basin SS exhibited enhanced efficiency, as compared to the pyramid SS and thus, it was selected for the experimentation [41] and the schematic arrangement of the test-setup with heat transfer through various locations is depicted in Fig. 3. A 4 mm thick transparent glass cover was used to enclose the SS from the top and its inclination angle was matched with the latitude of the experimental site (13.01° N) to receive the maximum available solar radiation and provided an optimum slope for the condensed water droplet to slide down and collect in the freshwater

measuring cylinder. The SS was made air-tight using a silicon sealant. A galvanized iron channel was positioned at the lower end of glass to accumulate the condensed water drops, which slide down from the glass cover. Three clean borosilicate glass cylinders of 1000 mL capacity with an accuracy of ± 2 mL were used to collect the freshwater output from the SS.

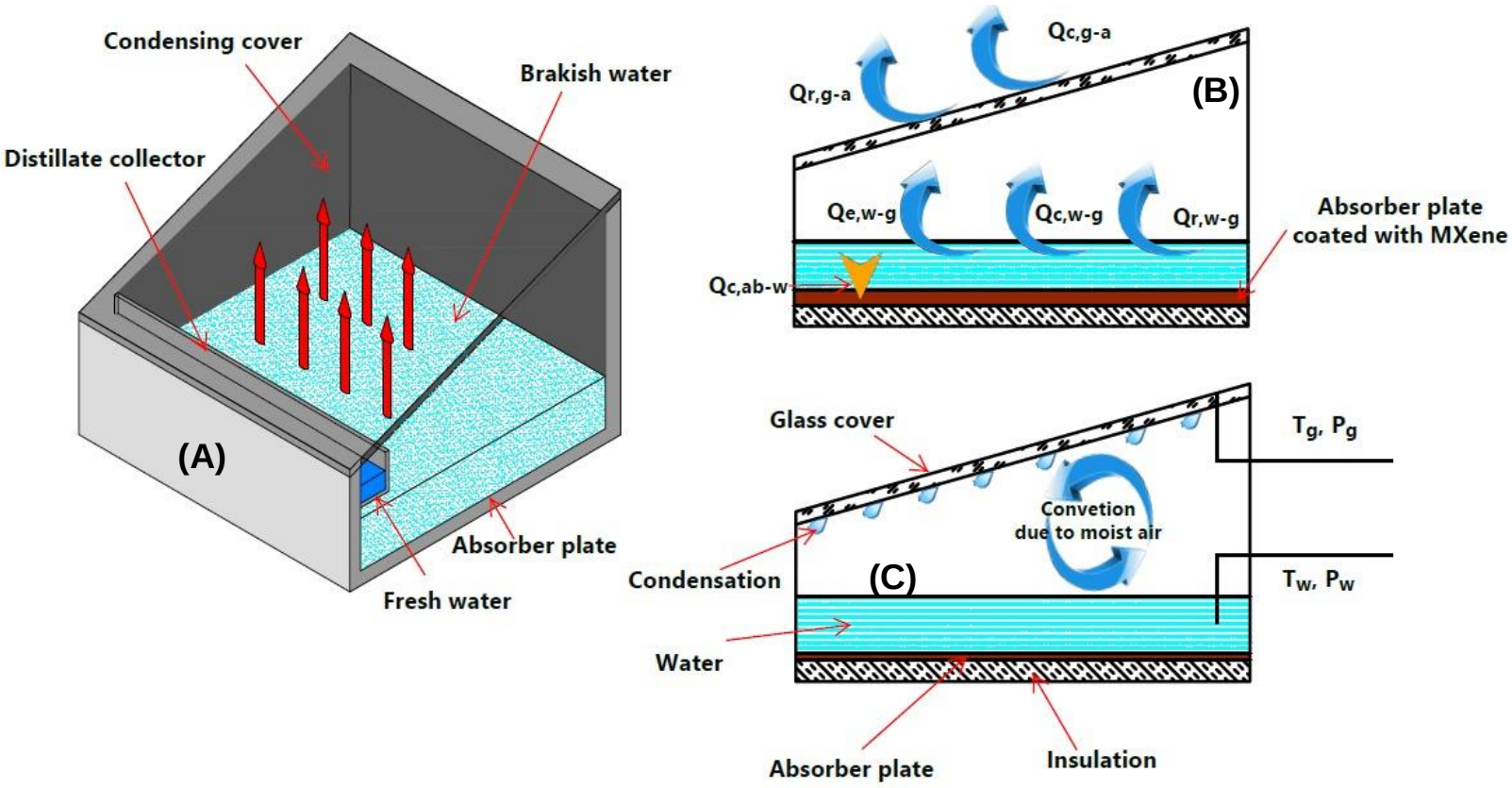

Fig. 3 (A) Schematic diagram of solar still with freshwater output, (B) Various heat transfer mechanisms inside the still between the absorber-water, water-glass and glass-air, (C) Condensed water droplet accumulation on glass owing to the mass transfer process by the natural convection of air.

Heat loss is a major concern of SS and it is adversely affected by the water productivity and thermal performance of the SS. Therefore, the SS should be very-well insulated to minimize the heat losses.

Nitrile foam sheet of 20 mm thickness was provided at the bottom of the SS and a 25 mm thick nitrile sheet was used for all side walls to minimize the heat losses from the SS. The brackish water was collected from an open well from an Industrial area in Tamilnadu, India (feed-water) and the SS was filled with the brackish water using 30 mm diameter opening created at the 'front-wall' of the SS. Each SS was filled with 13 liters of the brackish feed-water before the start of experimentation and they were refilled with the feed-water every half hour based on the distilled freshwater output of the respective SS. The quality of water produced is very important for a healthy lifestyle and the proposed device is well-suited for remote locations with low-cost fabrication, thus the distillated water quality should be examined to conclude that brackish water has been sufficiently purified and that it can be further used for drinking purposes. Therefore, the quality of the brackish feed-water and distilled freshwater (after the solar desalination) were examined using a pH meter (Hanna pH, ± 0.1pH), a total dissolved solids (TDS) meter (HM Digital TDS-3, ± 2 %) and an electrical conductivity meter (VKTECH, ± 2 %). A K-type thermocouple with accuracy = ± 1 ℃ and range of 0 ℃ - 100 ℃ was utilized to monitor the temperature of the absorber, water and glass cover. A solarimeter with accuracy = ± 10 W/m^2 and range of 0 W/m^2 to 2500 W/m^2 was utilized for measuring the solar radiation. The uncertainties involved in the measurement of length, width and thickness of the SS basin was determined by the equation, as follows:

$$\delta_D = \sqrt{(\Delta D_1 / D_1)^2 + (\Delta D_2 / D_2)^2 + ... + (\Delta D_n / D_n)^2} \quad (1)$$

where, D and ΔD are the minimum value and the range of deviation in the experimental parameters. The uncertainty in the aforementioned quantities are determined to be ± 0.5 mm.

Thermodynamic analysis of SS

In this section, the detailed thermodynamic equations used for determination of the energy performance of the SS with and without MXene coating of the absorber are presented.

The energy balance equation for the absorber can be written as follows [42],

$$I_t.\tau_g.\tau_w.\alpha_{ab} = h_{c,ab-w}\left(T_{ab} - T_w\right) + U_b\left(T_{ab} - T_{amb}\right) \quad (2)$$

The convective heat transfer rate between the absorber and water ($Q_{c,ab-w}$) is determined using the equation as follows,

$$Q_{c,ab-w} = h_{c,ab-w}\left(T_{ab} - T_w\right) \quad (3)$$

The convective heat transfer coefficient of water-glass ($h_{c,w-g}$) is determined using following equation [43],

$$h_{c,w-g} = 0.884 \times \left((T_w - T_g) + \frac{(P_w - P_g)(T_w + 273)}{268900 - P_w} \right)^{1/3} \quad (4)$$

where, P_w and P_g are calculated using following equation,

$$P_w = \exp\left(25.317 - \frac{T_w}{5144}\right) \quad (5)$$

$$P_g = \exp\left(25.317 - \frac{T_g}{5144}\right) \quad (6)$$

The evaporative heat transfer coefficient between water and glass is determined using the following equation,

$$h_{e,w-g} = 0.016 \times h_{c,w-g} \frac{P_w - P_g}{T_w - T_g} \quad (7)$$

The theoretical hourly water productivity (m_w) is determined using the following equation,

$$m_w = \frac{h_{e,w-g}.(T_w - T_g).3600}{L_{fg}} \quad (8)$$

The energy efficiency (η_{ene}) of the SS were determined using Eq. (9), [44]

$$\eta_{ene} = \frac{m_w \times L_{fg}}{I_t \times A_g \times \Delta t} \quad (9)$$

4. Results and discussion

4.1 Structural morphology of pure MXene (Ti_3C_2)

Three dimensional MAX phase (Ti_3AlC_2) was effectively converted into two-dimensional Ti_3C_2, which is clearly demonstrated in the SEM images presented in Fig. 4 (A-B). As seen in the images, the self-stacking layered micro-structure of Ti_3C_2 is clearly visible. The layer structure formation in MXene is owing to the 'domino effect' of the van der Waals forces between the two adjacent layers. The particle size ranged between 1 μm and 10 μm, and a similar layered structure was also reported by Ghidiu et al. [45].

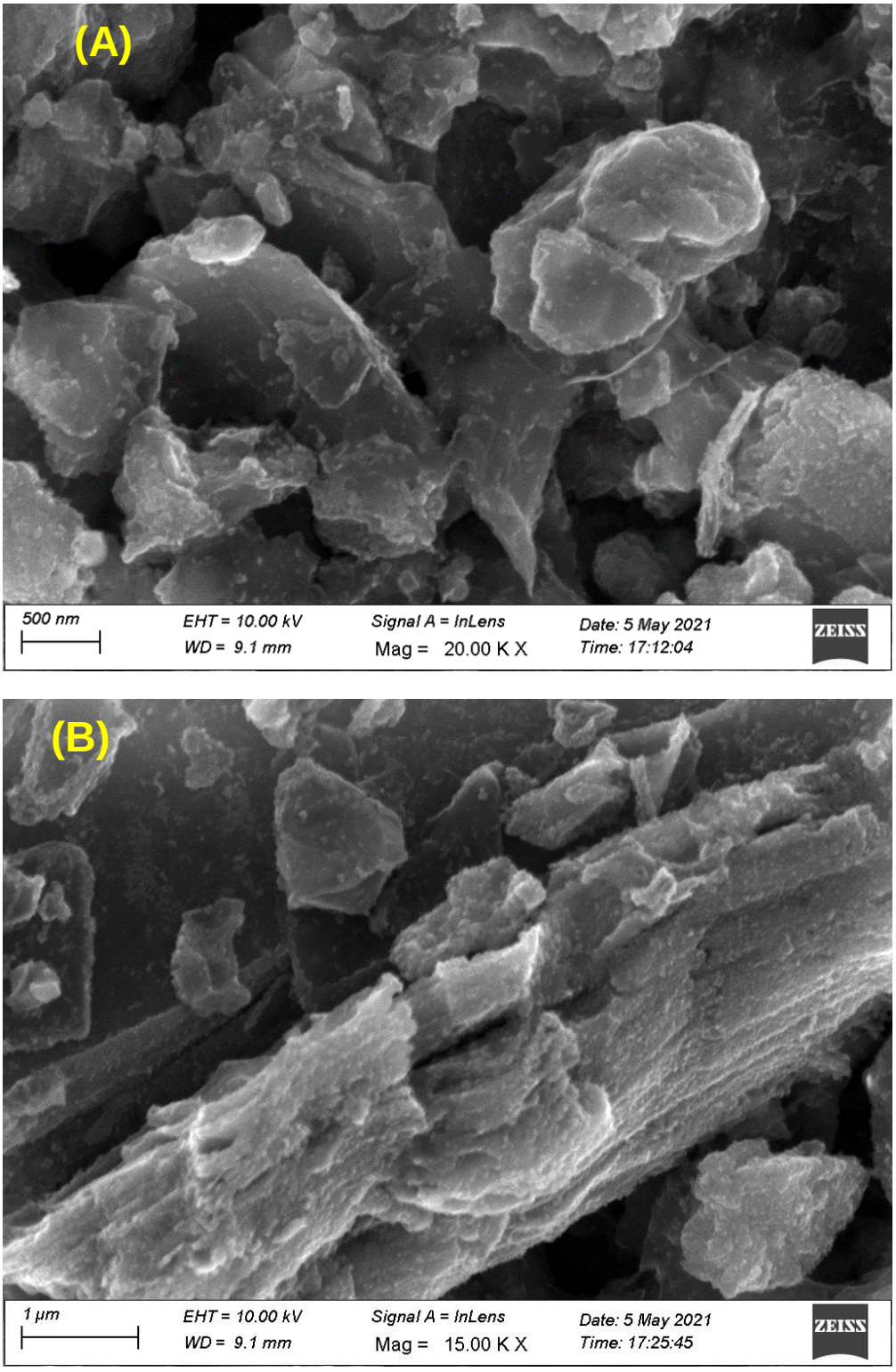

Fig. 4. SEM micrograph of as-synthesized MXene (Ti_3C_2) at magnification of (A) 500 nm and (B) 1 µm

The elemental mapping (EDX-mapping) of the pure MXene is presented in Fig. 5 (A-J), which clearly highlights the presence of Ti (61.7 %), C (8.6 %) and O (20.3 %) along with small amounts of F and a very meager amount of Al.

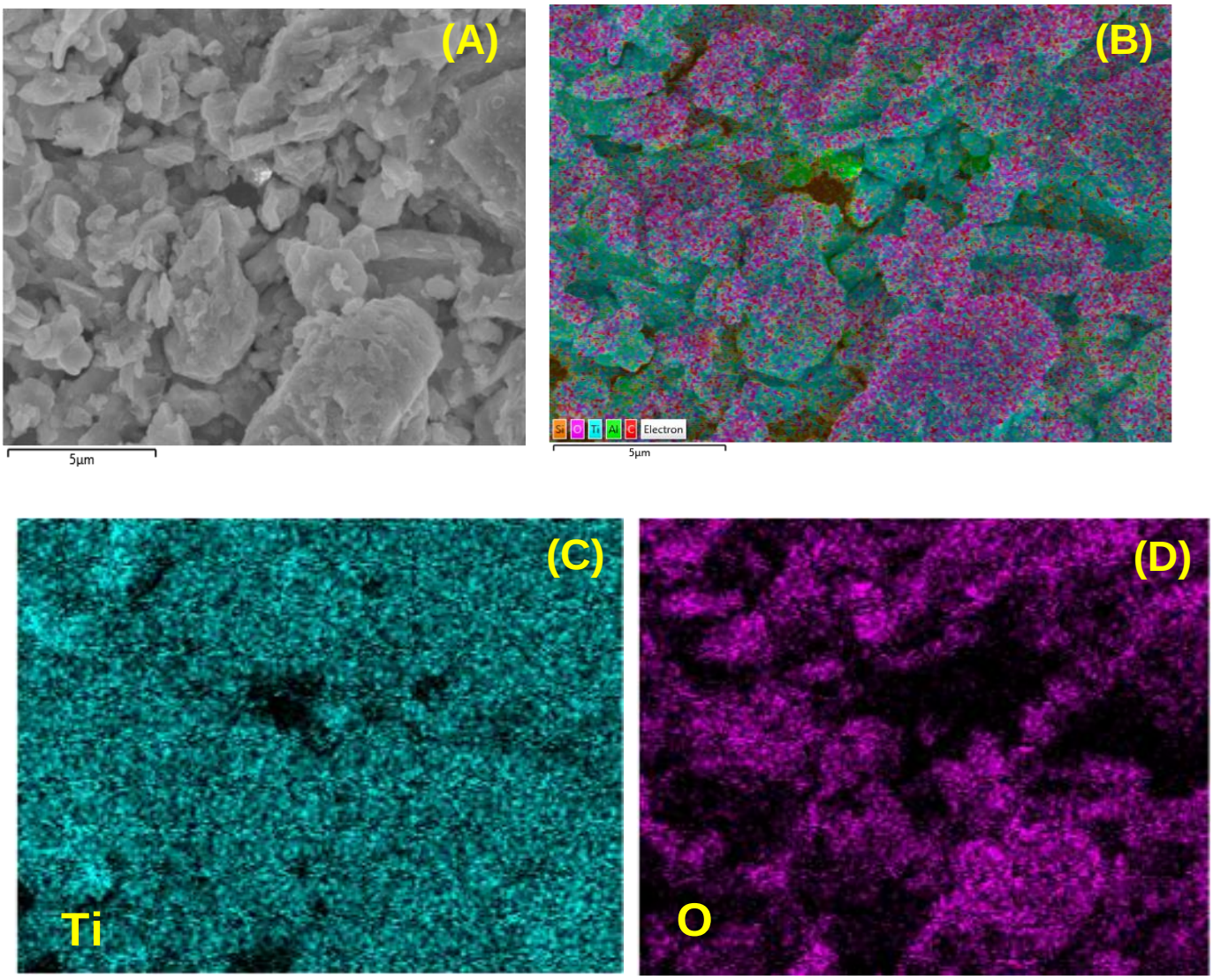

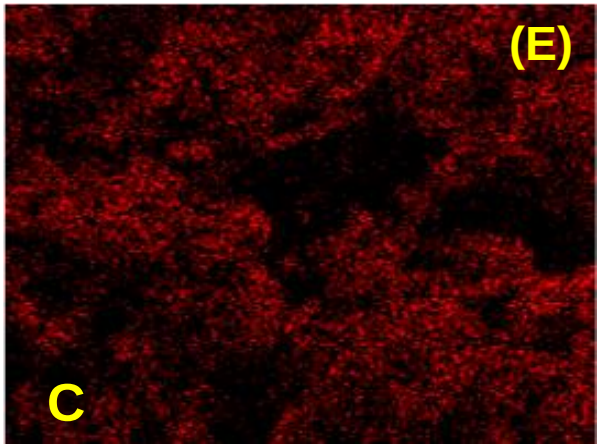
(E)
C

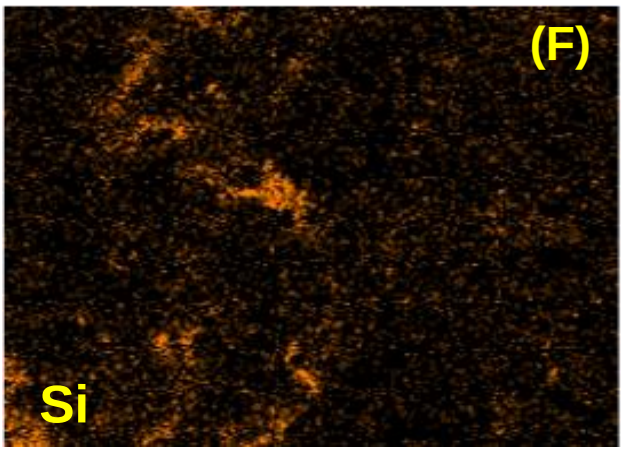
(F)
Si

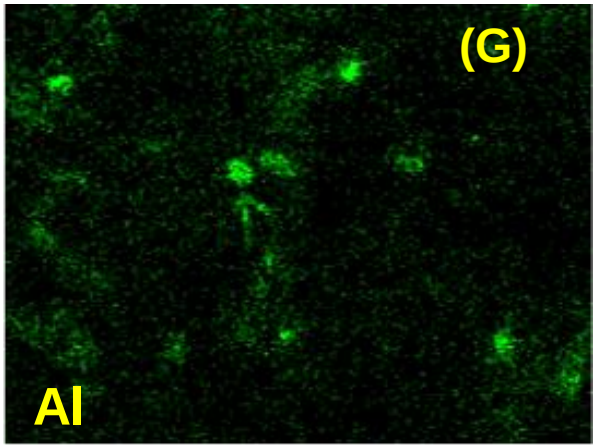
(G)
Al

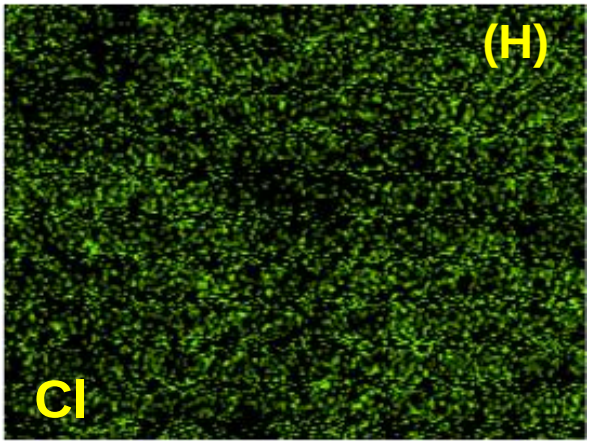
(H)
Cl

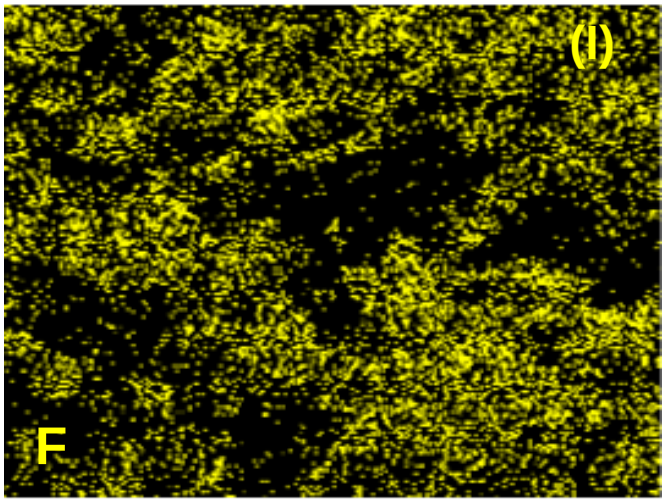
(I)
F

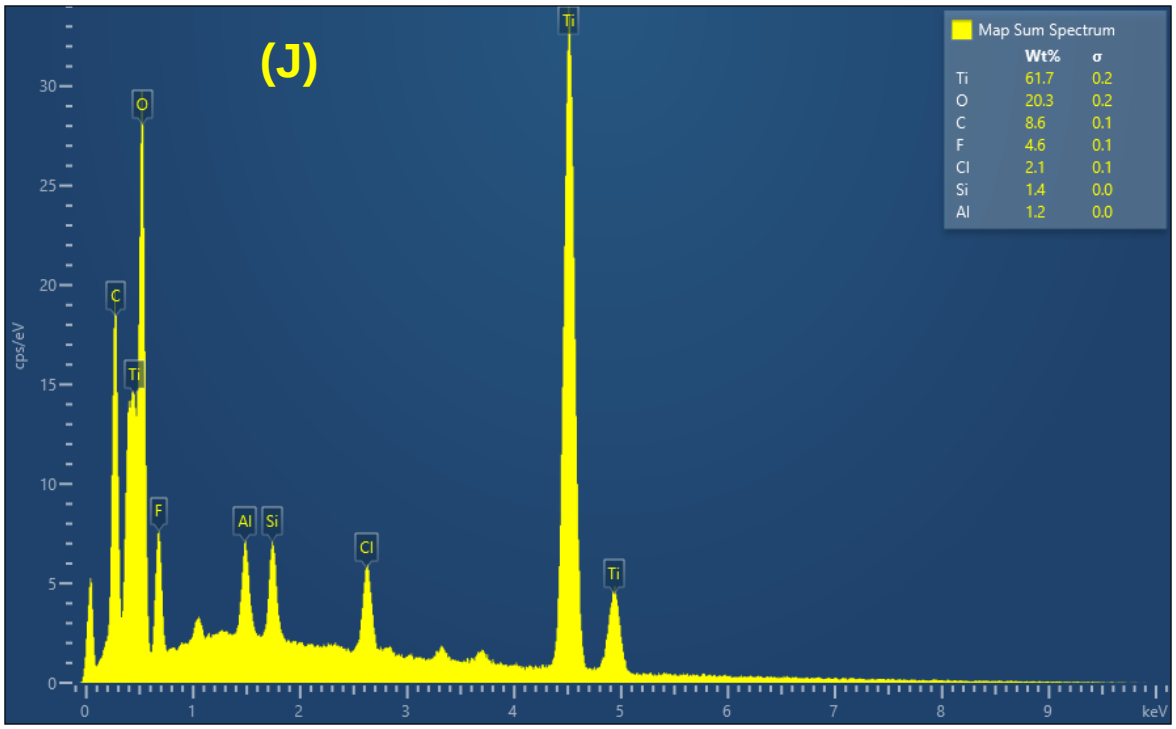

Fig. 5 (A–F) Color mapping images and (J) EDX analysis of as-synthesized Ti_3C_2 (MXene)

Fig. 6 depicts the XRD pattern of MXene, demonstrating the sharp diffraction peak at 7.1° (2θ) analogous to the (002) diffraction plane, leading to an interlayer spacing of 14.5 Å which is in accordance with published work of HCl fluoride salt etched Ti_3C_2 produced by Ghidiu et al. [45]. The other peaks at (004) and (008) also demonstrated the effective synthesis of MXene. Fig. 7 presents the TGA analysis of pure MXene for evaluating its mass decomposition under different temperature conditions. As shown in Fig. 7 under a nitrogen atmosphere, the weight loss in the first stage (room temperature to 200 °C) is ~ 6.9 %, owing to the losses of physically adsorbed water and hydrochloric acid from the MXene surface. The weight loss in the second stage of ~ 0.2 % in the temperature range of 200 – 800 °C (and ~7.1 % from room temperature to 800 °C) is mainly due to the loss of chemically adsorbed water, which is the OH groups attached on the surface of Ti_3C_2.

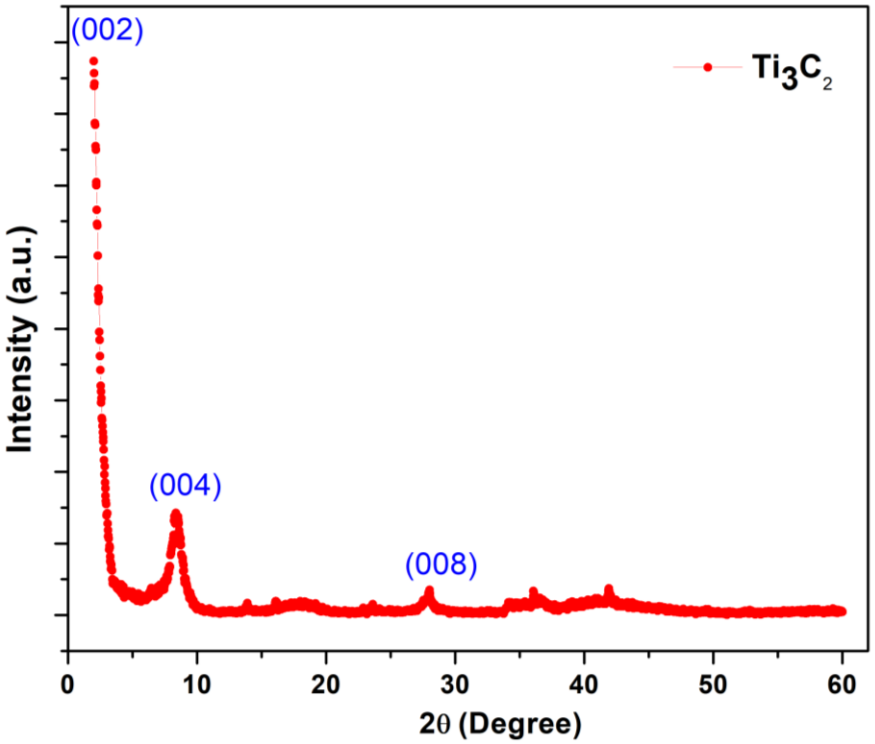

Fig. 6. XRD pattern of Ti_3C_2 (MXene)

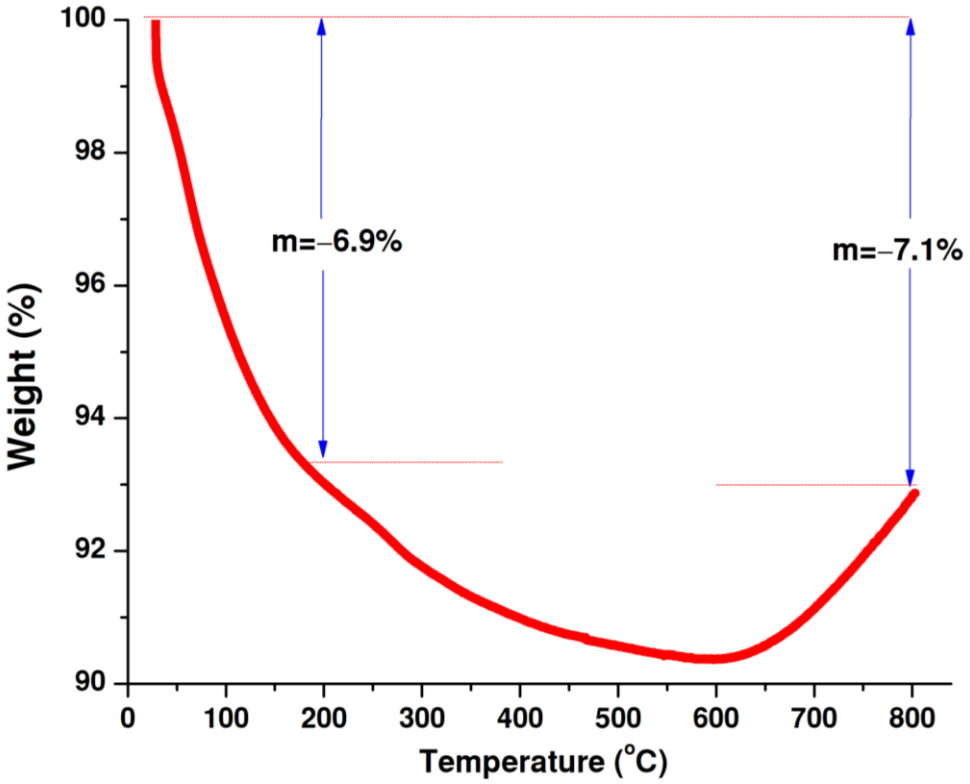

Fig. 7. TGA analysis of pure Ti_3C_2 (MXene)

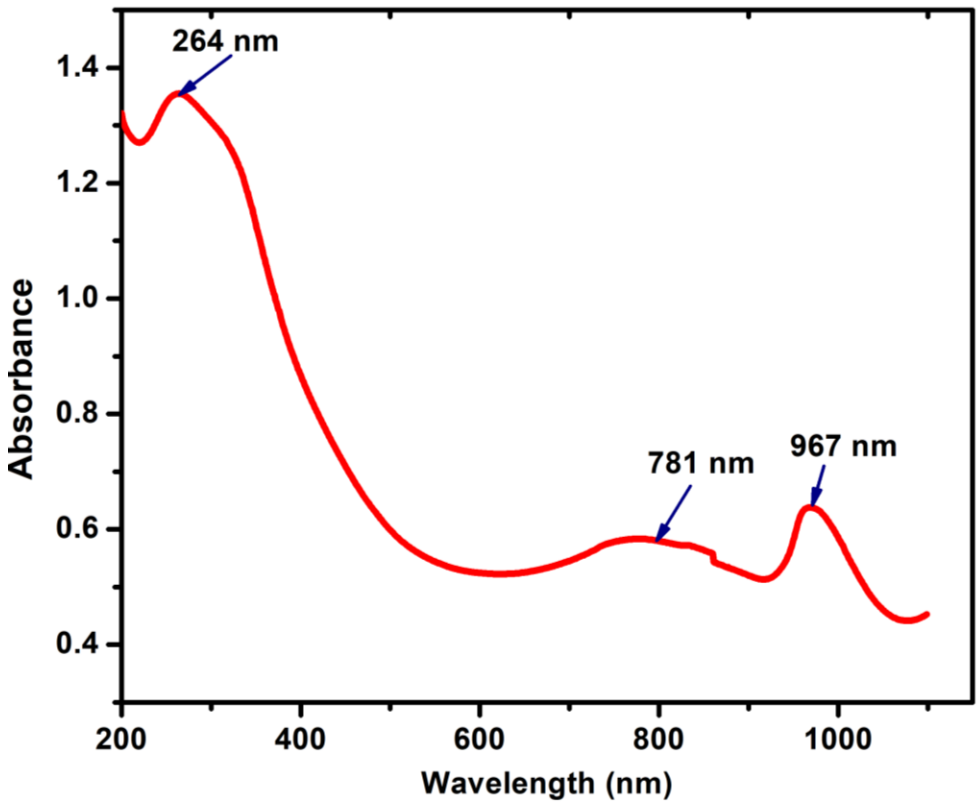

Fig. 8. UV-Vis absorption spectra of Ti_3C_2 (MXene powder)

Similar results of ~5 % weight loss from room temperature to 800 °C was reported for Ti_3C_2 by Li et al. [46]. It is inferred from the outcomes that the synthesized MXene is highly stable at high temperatures and thus is very suitable for high temperature application like solar absorber coating. Fig. 8 depicts the UV-Vis absorption spectra of powder MXene in range of 200-1100 nm and three peak are clearly observed in the image. The first peak was observed at 264 nm owing to the functional groups introduced during the synthesis MXenes and the next peak at 781 nm was seen due to the surface plasmon- nature of the MXenes. In addition, peak was also observed at 967 nm owing to the presence of water during the synthesis.

4.2 Thermal conductivity analysis of MXene/ Turpentine oil

The thermal conductivity of MXene dispersed in turpentine oil solution is a very imperative factor which directly influences the heat transfer behavior of the solar absorber during the operational

hours. Fig. 9 depicts the experimentally measured data of TC for the turpentine solution with two different mass concentrations of MXene (Ti_3C_2) by taking the average value of three measurements. The measured data reveals that the TC of bare turpentine oil is only 0.107 W/mK at 30 °C, which is in accordance with the value reported by Arani et al. [47]. The determined average error for three different measurement of bare turpentine oil was ± 0.05. The low error evidenced the accuracy of the TC measurement.

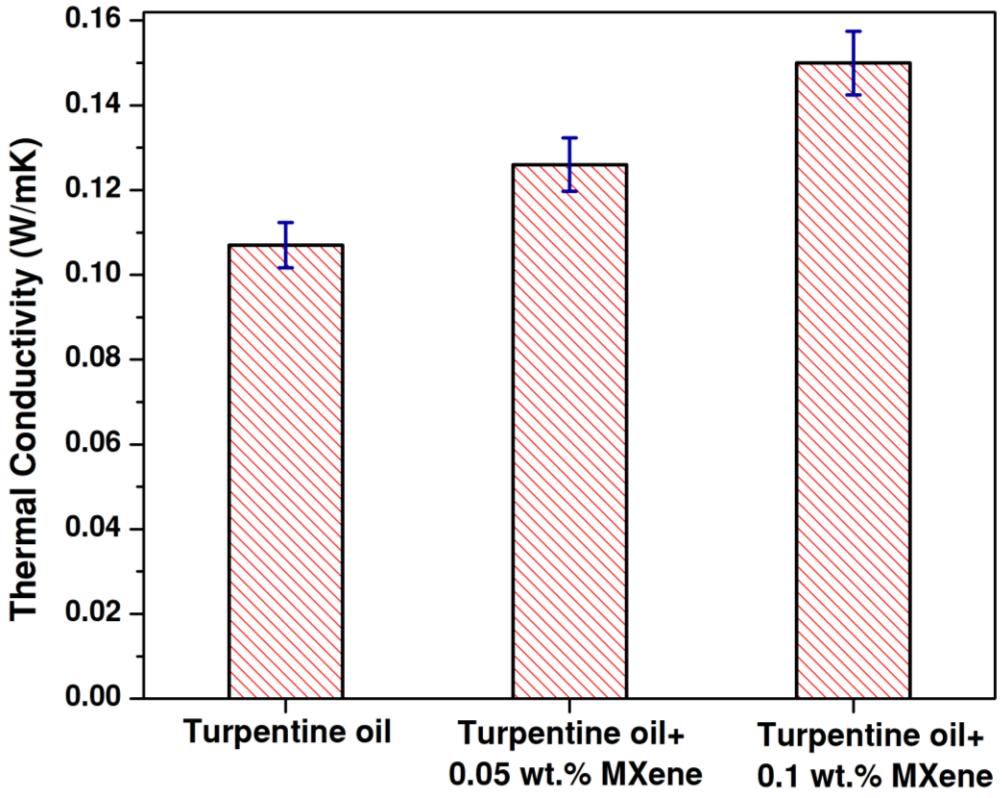

Fig. 9. Thermal conductivity of turpentine oil alone and with various MXene concentrations

Dispersion of 0.05 wt. % MXene in the turpentine oil increased the TC by 17.7 % and it was further increased to 40.1 % with increasing the loading of MXene to 0.1 wt. %, compared to the bare oil. The remarkably augmented TC with increasing the mass fraction of MXene could be owing to the excellent TC of MXene nano-flakes at high loading along with their excellent surface area to volume ratio. The unique two dimensional structure of MXene, could provide an excellent heat

percolating network, leading to remarkable improvement in the TC of the solution. It is also important to note that inter-flake thermal resistance (ΣR) of MXene cannot be neglected in the TC analysis owing to the existence of 'R' between the individual MXene flakes at the junction's along with the scattering of phonons between adjacent MXene flakes. Therefore, to increase the TC, ΣR should be reduced by improving the interaction between the MXene flakes. In addition, the synthesis route of MXene is also a critical parameter in improving the TC. Recently, a comparative study was reported on the role of MXene synthesis in the TC enhancement. Liu et al. [48] prepared Ti_3C_2Tx by selectively etching the Al from Ti_3AlC_2. In this work, multilayer un-delaminated Ti_3C_2Tx film was prepared, which retained more inherent connections between the MXene layers, leading to an enhanced TC of 55.8 W/m.K In contrast, Chen et al. [49] used a delaminated Ti_3C_2Tx nano-flakes based film and the TC was only 2.84 W/m.K (290 K). Similarly, our study also synthesized delaminated MXene and thus, further enhancement of the TC can be achieved by synthesis of un-delaminated MXene. However, in real-time applications, owing to several needs on the physical properties, it is critical to provide a balance among the multi-layer and delamination structures, as MXene delaminated flakes could provide several benefits like higher specific surface areas and capacitance [50]. It is also noteworthy that the viscosity of the base oil plays a vital role in providing the optimum path for heat transfer by provide excellent stability to the additives even under high temperature conditions. In contrast, turpentine oil possess very low viscosity and it is difficult to provide stability for the nanoparticle dispersion in this conditions. Therefore, our MXene loading is limited to a maximum of 0.1 wt. % and further investigation is required to explore the effect of increasing mass fraction of MXene on thermal conductivity enhancement with use of a suitable surfactant which could provide long term stability to the MXene in turpentine oil without compromising the thermal properties.

4.3 UV-Vis absorption spectrum analysis of MXene based paint

To effectively absorb the incident solar radiation and further store/supply it for heating the brackish water inside the SS basin, the solar absorber coating should exhibit excellent absorptivity and thus, the developed coatings were analyzed using UV-Vis absorption. Fig. 10 depicts the absorptivity analysis of the bare black paint and the black paint dispersed with two mass fractions of MXene. It was seen that the bare / conventional black paint exhibited an average absorptivity of 94.6 % with maximum and minimum values of 95.1 % and 94.1 %, respectively. Similar results of black paint absorption were also reported by Sharshir et al. [51].

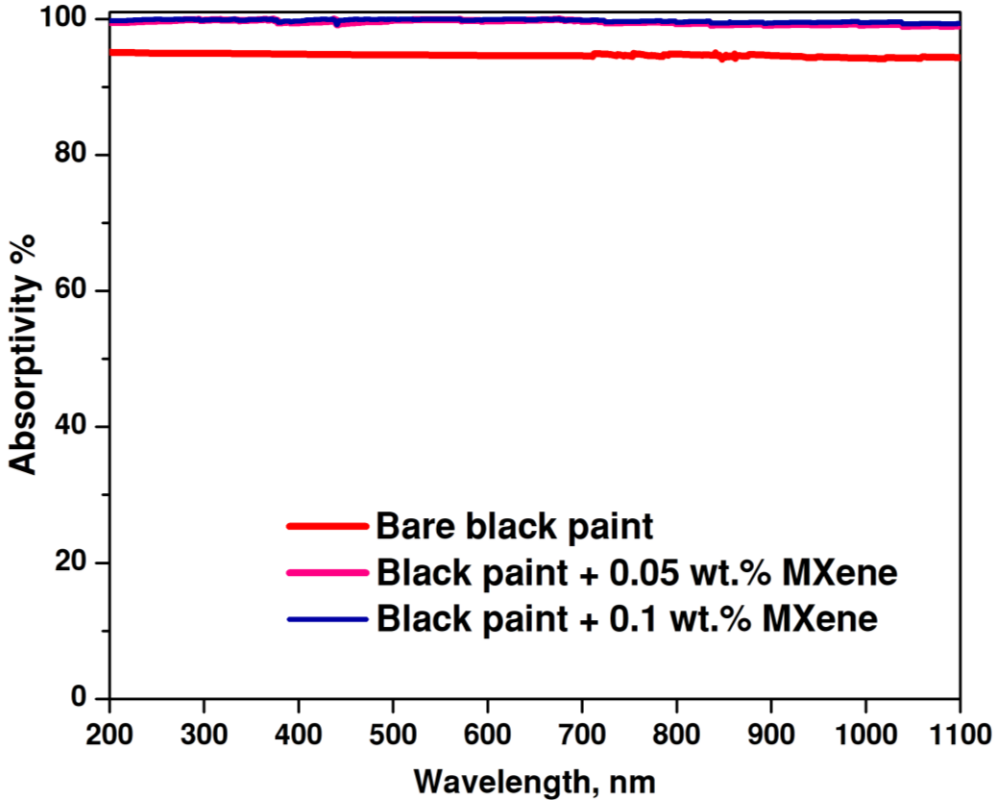

Fig. 10. Absorption spectra of the black paint without and with MXene at different wavelengths

With dispersion of 0.05 wt. % MXene (powder are black in colour) into the black paint, the absorptivity improved to 99.1 % (average) with maximum and minimum value of 99.7 % and 98.8 %, respectively. With further increase in loading of MXene to 0.1 wt. %, the average absorptivity

reached 99.6 % with maximum and minimum values of 99.9 % and 99.3 %, respectively. MXene possesses excellent solar-thermal absorption properties even at lower mass fraction, owing to its high surface area-to-volume ratio. With the incident solar radiation, simple harmonic oscillation of free electrons could be created by the plasmon, leading to exceptional light absorption. In previous work, it has been reported that even at 0.006 % MXene dispersion in base fluid, the transmittance of MXene based solution was close to 0 % under the full band with 97.66 % solar energy absorption [52]. It is worth understanding that with increased mass fraction of the MXene-nanoflakes in the solution, the scattering effect of the upper-layer of the solution improved considerably. Meanwhile, as per the Mie theory [53], owing to the large size of 2-D materials, the scattering effect increased, leading to a reduced transmittance and excellent absorption. However, it is advisable to explore and optimize the mass fraction to achieve the maximum solar absorptivity even with minimal loading of MXene for effective application of this material in solar-thermal technology.

4.4 Transient - temperature variation of SS

The temperature gain inside the still is a crucial factor in determination of the water yield of the desalination unit and therefore, assessment of this is required. The experiment was carried out on sunny day in May, 2021 and the temperatures of various junctions along with the solar radiation of the conventional SS is presented in Fig. 11 (A). As seen in figure 11, the irradiation increases during the morning hours and achieves a maximum value of 998 W/m^2 at 1 PM. After noon, the radiation reduces and reaches a minimum value of 413 W/m^2 at 5 PM. The average solar radiation was found to be 735 W/m^2 during the experimental hours. It is interesting to note that the availability of solar radiation was about 12 hours in the experimental days, however potential availability of the sunshine hours (>200 W/m^2) is only 8 - 10 hours over the year. Therefore, to

assess the desalination unit performance effectively, the experimental hours were selected from 9 AM to 5 PM. The ambient temperature mainly depends on solar radiation and follows a similar trend. Maximum ambient temperature was found to be 35.8 °C (1 PM) and the average temperature during experimentation was 33.7 °C. The peak temperature inside the still was exhibited by the absorber, followed by the water and glass temperatures. The G.I bare black paint coated solar absorber possesses excellent thermal conductivity and absorbs the significant incident radiation, leading to storage of a large percentage of the available solar energy which helps in increasing the water temperature. The peak temperature of the absorber and water were 66.1 °C and 63 °C respectively at 1 PM, as illustrated in Fig. 11 (A). With the increase in water temperature, evaporation starts and the vaporization of water initiates. This evaporated water condensate onto the glass and increases its temperature. The maximum temperature of the glass was found to be 52 °C at 1 PM.

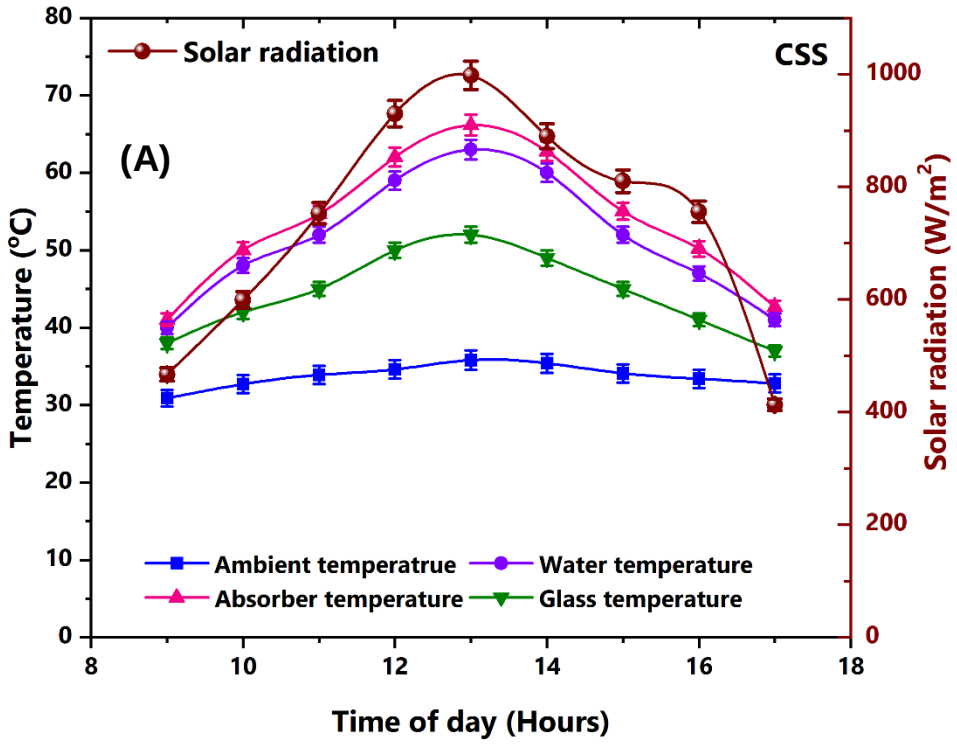

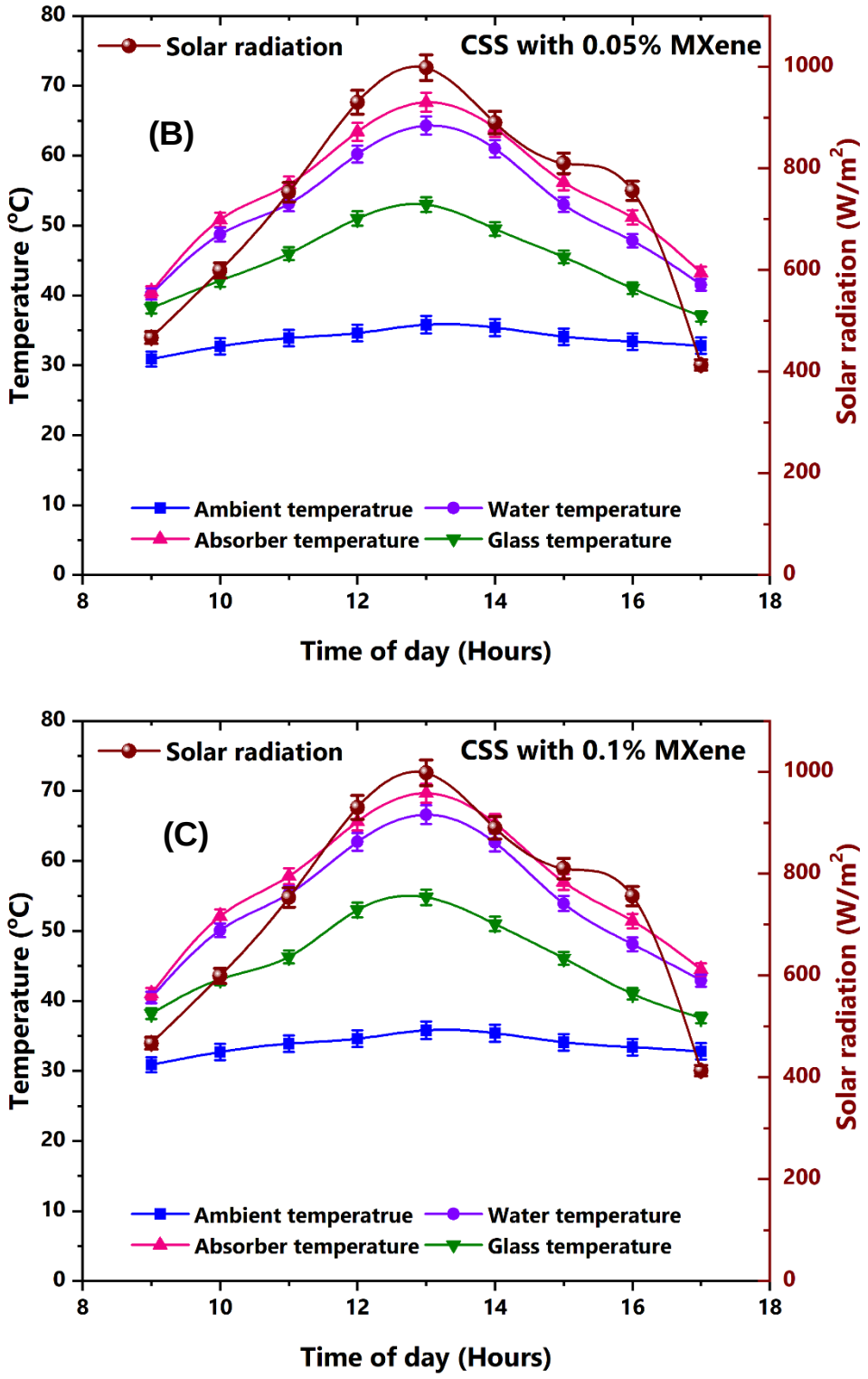

Fig. 11. Solar radiation and temperature variations with time for (A) conventional SS, (B) Conventional SS with 0.05 wt. % MXene, (C) Conventional SS with 0.1 wt. % MXene.

The objective of this work is to explore the role of MXene in improving the thermal performance of the desalination unit and thus, MXene was mixed with black paint and coated onto the absorber to increase the overall performance of the desalination unit and its influence on water and glass temperature is presented in this section. Fig. 11 (B) depicts the hourly temperature variation in the desalination unit with 0.05 wt. % MXene coated absorber. With MXene loading in the paint coating, the peak temperature of the absorber increased and reached a maximum value of 67.2 ℃ at 1 PM. The enhancement is attributed to the increased solar-absorption behavior with improved conductivity of the MXene coated absorber. It possesses phenomenal thermal conductivity and the nano-flakes of MXene with 2-D structure provided excellent scattering effect, which in turn reduces the transmittance and provides superior absorption, leading to higher gain in the temperature. With improved peak ambient temperature, the water temperature also increased and reached a peak of 64.3 ℃ at 1 PM. Higher water temperature is always beneficial in promoting faster evaporation, leading to an improved peak glass temperature of 53 ℃ at 1 PM. Increasing loading of MXene to 0.1 wt. %, the absorber temperature increased significantly and reached a peak of 69.6 ℃ (1 PM), as presented in Fig. 11 (C). It could be due to the higher heat network with increased MXene loading that provides improved heat transfer and also increases the absorptivity of the absorber. Similar, the water and glass peak temperature also improved and reached peak values of 66.6 ℃ and 54.8 ℃ respectively at 1 PM.

Fig. 12 (A) presents the hourly variation in temperature difference between the water and glass for all three SS. It is well-known that the temperature difference between the water and glass plays a significant role in promoting higher heat transfer, leading to improved water yield. As can been seen in figure 12 (A), the temperature difference was low in the early experimental hours, owing to the gradual heating of water with respect to the solar radiation, and it attained a peak

value at 1 PM. With the MXene coated absorber, there was a noteworthy rise in the water temperature, leading to an improved temperature difference between water and glass. The SS with the 0.1 wt. % MXene coated absorber exhibited a peak temperature difference of 11.8 °C (1 PM), whereas it was 11.5 °C and 11 °C respectively, for the SS with 0.05 wt. % MXene and the bare black paint coated SS. The average full-day temperature difference between the water and glass was also higher (7.95 °C) for the SS with 0.1 wt. % MXene, as presented in Fig. 12 (A). This could be attributed to the improved heat supplied by the superior solar absorption of MXene along with the higher thermal conductivity and large 2-D flakes, which promoted improved heat transfer from the absorber to the water, which in turn provided a higher temperature difference between the water and glass.

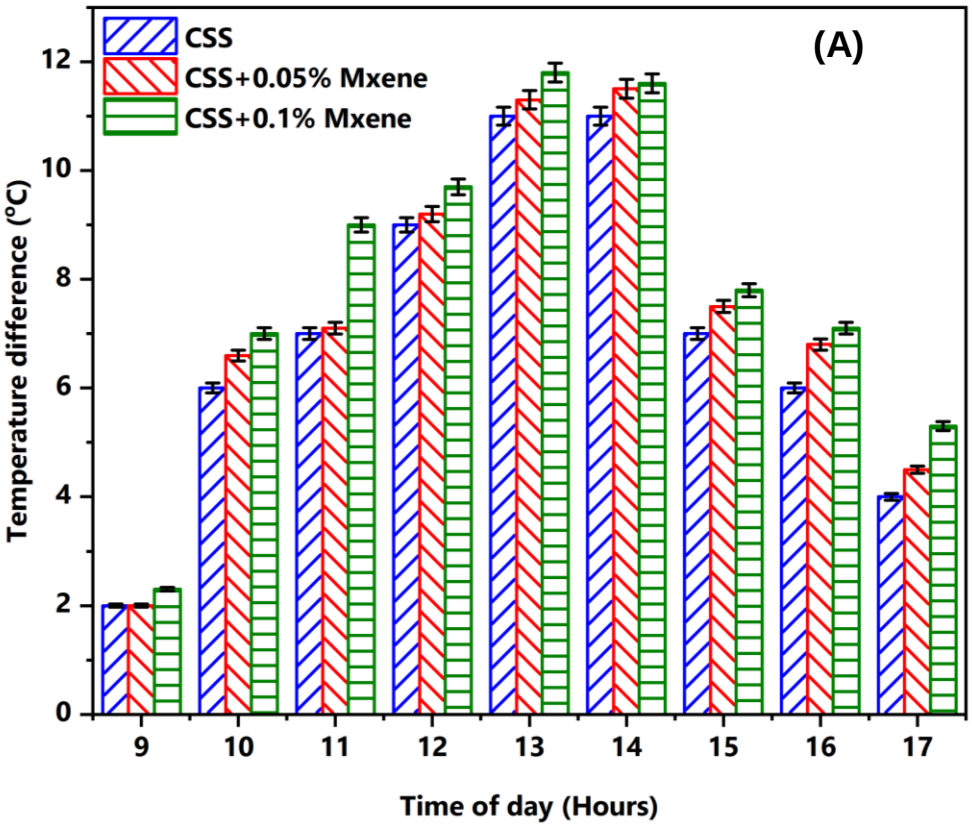

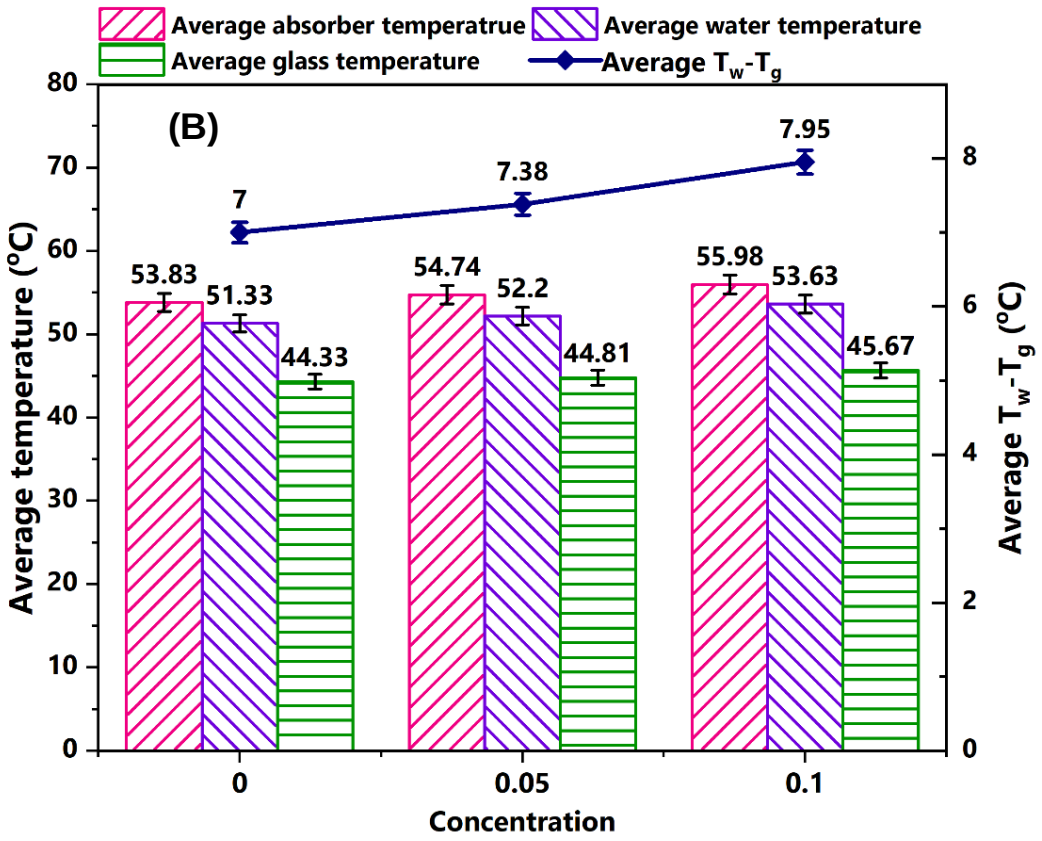

Fig. 12 (A). Hourly variation in temperature difference between the water and glass for the three SS, (B) Average full-day temperature of absorber, water and glass of SS without and with 0.05% and 0.1% MXene coated absorber.

The CSS with 0.05 wt. % MXene exhibited an average full-day temperature difference between the water and glass of 7.4 °C, whereas it was only 7 °C for the CSS with bare black paint coating. It is also noteworthy that higher loading of MXene could adversely affect the durability of the coating owing to the non-uniform dispersion of the MXene in the paint solution, which could lead to peeling of the MXene coating from the absorber after repeated operations of the SS. Therefore, only a small fraction of MXene is chosen in this work for providing long-term durability to the absorber, and it is suggested to further optimize the mass fraction of MXene to achieve long term enhanced performance of the desalination unit for water heating/purification purposes.

Fig. 12 (B) also depicts the average full-day temperature of the absorber, water and glass. The average full-day maximum temperature of the CSS absorber with bare blank paint was 53.83 °C, which was augmented by 1.7 % and 4 % respectively, with MXene coating of 0.05 wt. % and 0.1 wt. %. It is obvious that improved conductivity with significant solar absorptivity provided the optimum heat transfer to the MXene coated absorber, which helped in improving the full-day average temperature. As the increased absorber temperature provided heat to water and increased its temperature, a similar trend was also shown by the water. Average full-day temperatures of 53.63 °C, 52.2 °C and 51.3 °C were exhibited by CSS-0.1 wt. % MXene, CSS-0.05 wt. % MXene, and bare black paint coated CSS, respectively.

4.5 Thermodynamic analysis and water yield analysis of the SS

To assess the role of MXene on heat transfer enhancement inside the basin of the desalination unit, detailed thermodynamic analysis was carried out and is presented here along with the water yield data. Fig. 13 (A) demonstrates the average convective heat transfer coefficient and heat transfer rate between the absorber and water of the SS, determined using equations (2-3). As seen from the figure, the average convective heat transfer coefficient was 167.08 W/m^2k for the bare black paint coated CSS and it was significantly augmented by 45.73 % with 0.05 wt. % of MXene. It is obvious that the convective heat transfer coefficient mainly depends on the temperature difference between the absorber and water and the temperature difference between the absorber and the ambient air. MXene has remarkably improved the absorption properties, leading to significant improvement in absorber temperature, which leads to the noteworthy improvement in the convective heat transfer coefficient. With a further increase in loading of MXene to 0.1 wt. %, the average convective heat transfer coefficient augmented by 46.81 %, compared to the black painted CSS. It is interesting to note that the increased heat transfer coefficient between the absorber and water provided a higher

evaporation rate and leads to augmented water yield. The average convective heat transfer rate, as calculated from equations (2-3) also exhibited a similar trend, and the absorber with 0.1wt. % MXene exhibited higher average convective heat transfer. The average convective heat transfer rates were 199.71 W, 210.58 W and 237.99 W for CSS, CSS-0.05 wt. % MXene, and CSS-0.1 wt. % MXene, respectively. The hourly variation in convective heat transfer rates are plotted in Fig. 13 (B), which highlights the variations in convective heat transfer. It was seen that the peak value of heat transfer rate occurred at 1 PM for all three cases. It is well-known that the heat transfer rate mainly depends on the heat transfer coefficient along with the temperature difference between the absorber and water. The MXene coated absorber has an improved heat transfer coefficient, leading to improvement in hourly convective heat transfer rate, relative to the CSS. The maximum hourly values of the heat transfer rates were found to be 263.17 W, 277.32 W and 282.76 W for CSS, CSS-0.05 wt. % MXene, and CSS-0.1 wt. % MXene, respectively. Table 1 presents the comparison between the heat transfer coefficients for all three SS. The heat transfer coefficient (convective and evaporative) from water-glass are determined using equations (4-7). As seen in Table 1, MXene provided a higher heat transfer rate for convection as well as evaporation and led to augmented heat transfer rates. The water inside the basin reached an elevated temperature with increasing loading of MXene that provides more heat through the absorber and promotes higher convection and evaporation between the water and the glass.

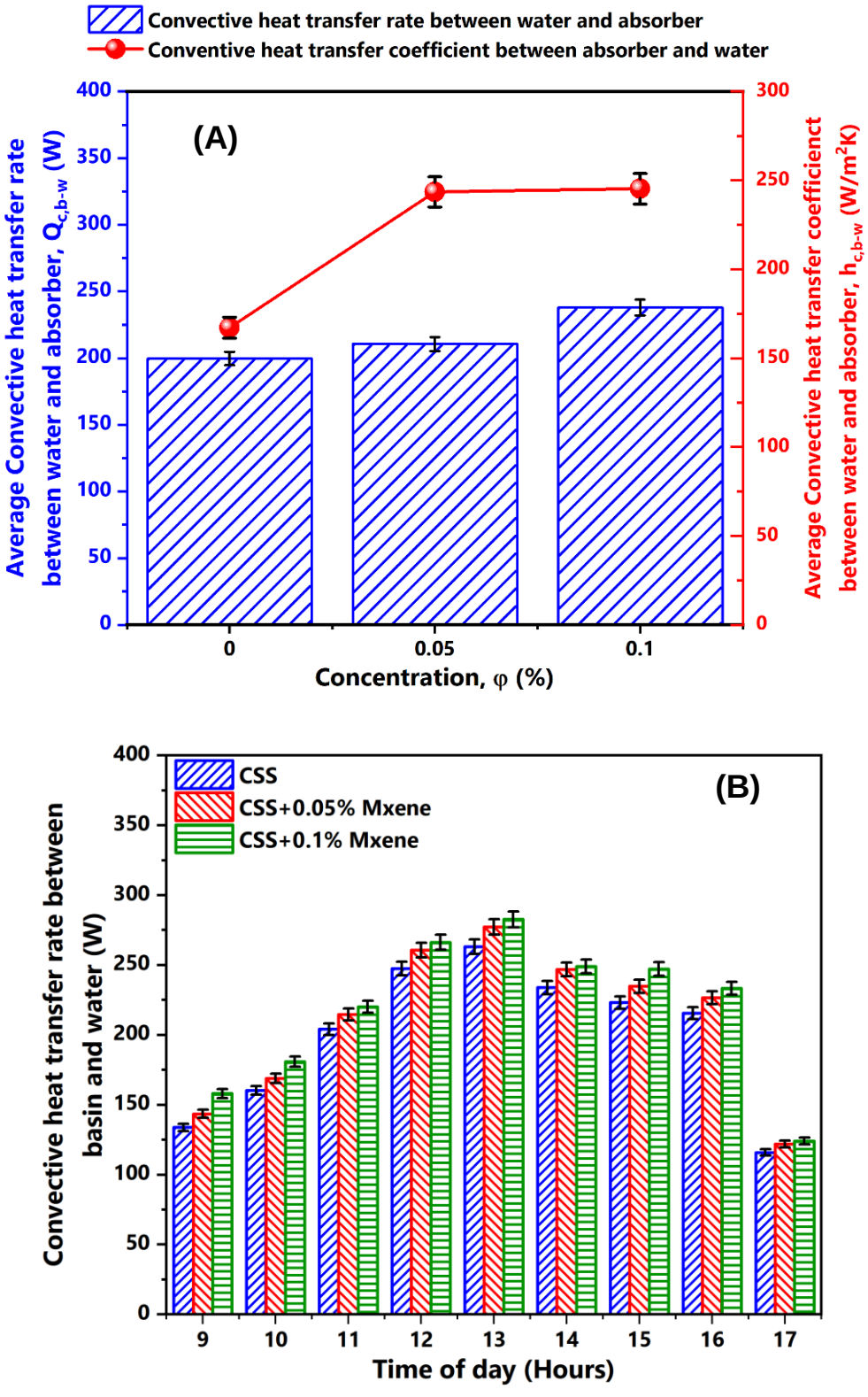

Fig. 13 (A) Average convective heat transfer coefficient and convective heat transfer rate, (B) Hourly convective heat transfer between absorber and glass of the three SS

The heat transfer coefficients significantly improved with increasing loading of MXene in the absorber, which is predominantly due to the excellent solar absorptivity and higher thermal conductivity of the MXene coating on the solar absorber.

Table 1. Comparison of average heat transfer coefficients (W/m^2 K) between absorber (ab) and water ($h_{c,ab-w}$), and between water and glass ($h_{c,w-g}$ and $h_{e,w-g}$) and for the three different SS.

Type of SS	**Average $h_{c,ab-w}$**	**Average $h_{c,w-g}$**	**Average $h_{e,w-g}$**
Conventional SS	167.08	1.66	31.61
CSS-0.05 wt. % MXene	243.5	1.69	33.28
CSS-0.1 wt. % MXene	245.3	1.74	36.21

Fig. 14 compared the theoretical water yield calculated using equation (8) to the experimentally collected water yield (actual). In experimental yield analysis, owing to the lower solar radiation in the early part of the experimental, the water yield was only 110 gm at 10 AM. With the increase in solar radiation, water yield increased and reached a peak value of 420 gm at 1 PM. Later, with reduction in solar radiation, then value of water output also reduced. The full day water yield was found to be 1.84 kg for the conventional SS. With the dispersion of 0.05 wt. % MXene into solar absorber coating, the absorption behavior along with the thermal conductivity of the absorber increased, leading to enhanced water temperature and evaporation rate. This increased the water yield of the modified SS coated with MXene. It was found that the SS coated with 0.05 wt. % MXene exhibited a maximum water yield of 480 gm at 1 PM and the full day water yield was 1.95 kg. With further increase in the loading of MXene to 0.1 wt. %, the maximum water yield reached 570 gm and the full-day water yield was 2.07 kg.

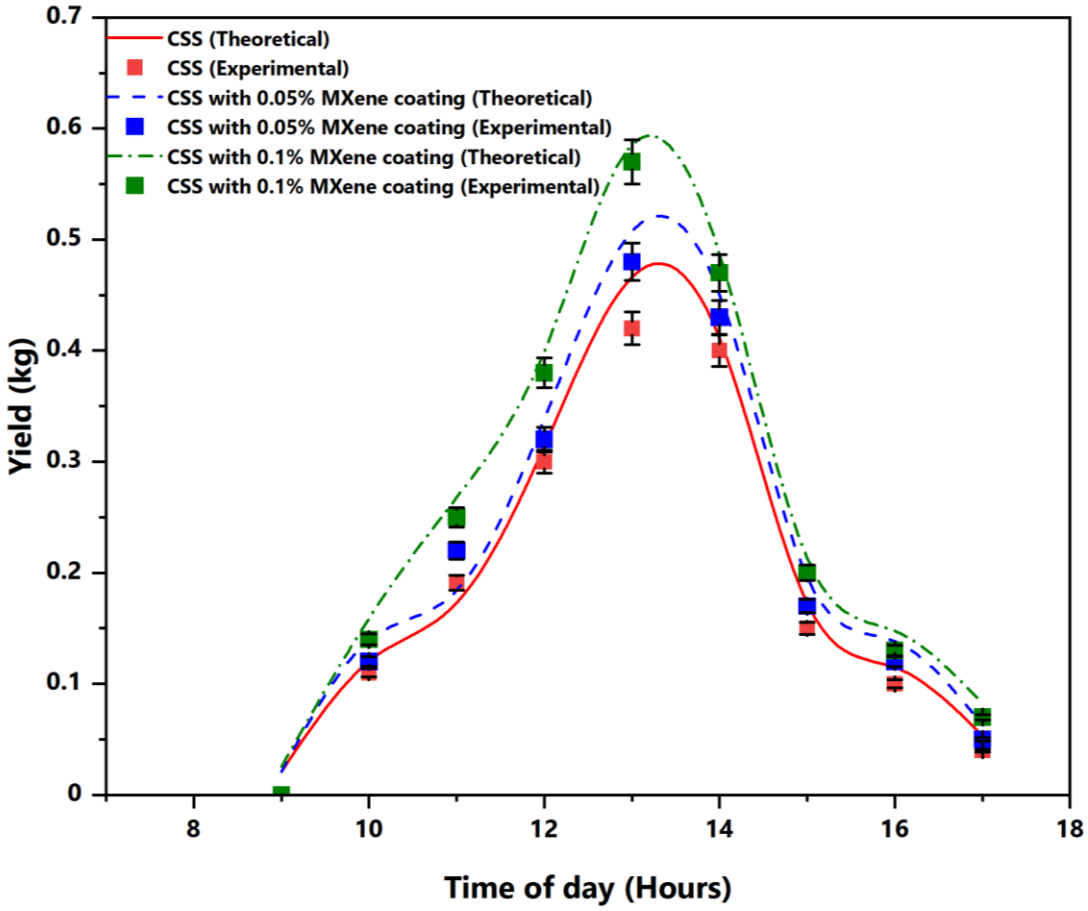

Fig. 14. Theoretical water yield in comparison with the experimentally determined yields of the three SS.

The significant augmentation in water yield with the MXene coating could be due to the higher conductivity and superior solar absorption characteristics of Mxene, which improved the heat transfer rate and provided higher water vaporization. The fascinating features of MXene with its excellent thermo-physical properties and novel 2-D structure has provided significant augmentation in water yield with a minimal mass of MXene, and the developed solar absorber can be effectively used for other solar heating applications also to improve the overall thermal performance of the system. In addition, the theoretically calculated water yields were found to be identical to the actual experimental yields for the MXene coated SS, with the overall deviation of ± 5%, demonstrating the accuracy of the thermal modelling.

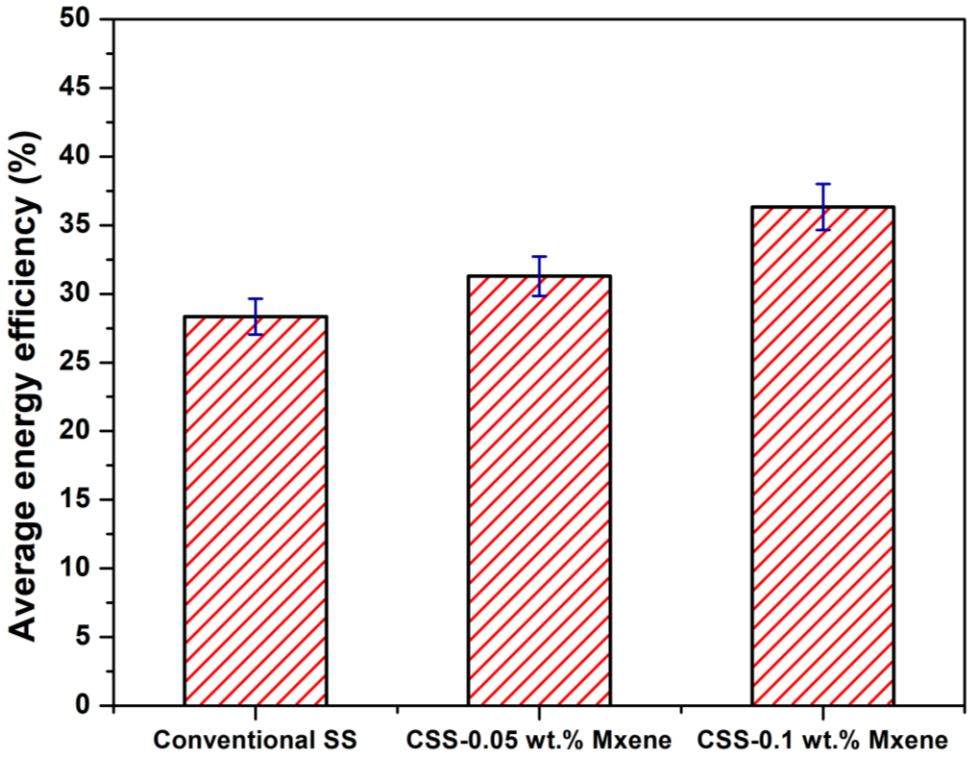

Fig. 15. Average energy efficiency of the three SS.

Fig. 15 depicts the average energy efficiency of the solar desalination units calculated using equation (9), which mainly depends on the water yield. As seen in figure 15, the bare black paint coated absorber based SS exhibited an average energy efficiency of only 28.33 %. With MXene loading of 0.05 wt. % in the absorber coating, the average energy efficiency was augmented by 10.5 % (to 31.28 %), compared to the CSS. Higher water yield generation due to the improved water evaporation and heat transfer rate along with the excellent solar-absorption by the MXene coated absorber provided the higher energy efficiency. Loading of MXene plays an important role in augmentation of the energy efficiency and with a further increase in MXene loading to 0.1 wt. %, the energy efficiency increased by 28.16 % (36.31 %) compared to the CSS. It is concluded from the results that the novel 2-D structure with excellent thermo-physical properties and superior solar absorption characteristics of MXene has provided higher heat transfer rates and increased evaporation, which leads to improved water yield and overall thermal performance of the solar

desalination unit. In addition, as proven herein, the MXene based coating can be highly beneficial in solar thermal applications such as solar collectors and receivers for increasing the system performance even with minimal loading of MXene. With its exceptional properties and the significant improvement in overall system performance using MXene, its applications in solar-thermal can bring astonishing outcomes and help in demonstrating the effectiveness of this material.

5. Water quality analysis

The quality of available water is a very important factor in providing health and maintaining good hygiene to the population and thus, the drinking water quality resulting from the solar desalination processes must be assessed to ensure that it is suitable for drinking. The present work measured the pH, total dissolved solids (TDS) and electrical conductivity of water to compare the water before and after distillation. Brackish feed-water collected from an Industrial area open-well exhibited TDS of 930 ppm and this was drastically reduced to 17 ppm after the distillation. The outcomes show that the TDS is well within limit of the WHO acceptable range (< 300 ppm) [54]. Similarly, the pH of the brackish feed-water was 6.4 and it reached 7.4 after the desalination (WHO acceptable range =6.5-8.5) [55]. The electrical conductivity of the brackish water was 860 μS/cm and it reached 38 μS/cm after the desalination (WHO range = 0-800 μS/cm) [56]. It is inferred from the water quality measurements that all the water parameters are well within the acceptable limits after the desalination of brackish water and it could be used for drinking purposes.

6. Societal contributions and limitations and future recommendation

With escalating population and global warming, renewable energy based technologies can be the most important factors in reducing emission and global warming. In this regard, the solar based desalination particularly solar still with augmented water yield by utilizing MXene can pave the

way in decreasing the dependency on high grade energy based desalination processes such as reverse osmosis and membrane based system. As the system is completely solar-driven, it can be easily installed in remote areas having excellent solar radiation throughout the year like Indian states of Rajasthan and Gujarat. This device can fulfill the water needs to a small family with minimum freshwater cost by converting the locally available brackish water or even sea water. In addition, compared to all the desalination plants where large initial investment is needed, the proposed distillation unit requires a very low investment for its operations and a non-skilled operator. With recently concluded annual UN climate change conference 'COP26', a stronger emissions reduction targets was fixed by 2030 and thus, to match the objective of 'COP26', solar driven desalination with excellent energy efficiency and heat transfer behavior by using MXene as novel material can be a potential solution to fulfill the freshwater demands of the developing countries with abundant solar energy availability with minimal investment.

Although, the solar energy based desalination system can be effective utilized in emission reduction and freshwater generation, the major concern of this devices is 24-hours operations. As the solar energy is intermittent in nature, the operation of device can be completely restricted as per the ambient conditions. In addition, the MXene production is still limited to laboratory scale and it requires the state of the art facilities for its synthesis. Therefore, the cost of MXene could limit its application. Moreover, with increasing demand and application of this materials, its price could be drastically reduced similar to graphene based materials and with the exceptional thermal and physical properties of MXene, the proposed unit could be a game changer in the field of water purification. In the view of intermittent nature of solar driven desalination devices, usage of energy storage materials like phase change material in the form of paraffin wax with the doping of MXene could be solution to store the excessive available energy during the peak hours and then, use it

during the off-peak hours to get the desired water temperature required for evaporation even during the low solar radiation intensity. By the synergetic usage of phase change material and absorber coating using MXene, the overall water production cost could be increased and even night time production of water can be achieved using these approaches. In addition, the un-delaminated preparation can leads to superior enhancement in thermal conductivity as compared to delaminated MXene and thus, it is suggested to explore the effect of un-delaminated structure on thermal conductivity and solar absorption behavior of MXene

7. Conclusion

The effect of MXene coating (0.05 wt. % and 0.1 wt. %) of the absorber on the thermal performance and water productivity of the solar desalination unit is experimentally examined. Firstly, 2-D MXene (Ti_3C_2) was prepared from 3-D MAX phase and SEM analysis demonstrated multilayer structure of MXene with particle size ranging between 1 μm and 10 μm. XRD analysis confirmed the purity of the prepared MXene and TGA demonstrated excellent stability. Thermal conductivity of turpentine oil improved by 40.1 % with MXene loading of 0.1 wt. %, whereas average solar absorptivity reached 99.6 %. Our results demonstrated excellent water output of 2.07 kg using 0.1 wt. % MXene doped in black paint coated SS absorber, however the conventional SS with only black paint coating exhibited only 1.84 kg water output. The heat transfer coefficient and heat transfer rate between absorber-water and water-glass were significantly augmented with increasing MXene loading. The average energy efficiency of the coated absorber still with 0.1 wt. % MXene was augmented by 28.16 % compared to the bare SS with only black paint coating. Water quality study confirm that generated freshwater after distillation was well within the acceptable range as prescribed by the World Health Organization.

CRediT authorship contribution statement

Amrit Kumar Thakur: Conceptualization, Methodology, Validation, Formal analysis, Investigation, Writing - original draft, Writing – review & editing. **Ravishankar Sathyamurthy:** Conceptualization, Investigation, Resources, Data curation, Writing - review & editing, Supervision. **R. Saidur:** Writing - review & editing, Supervision, Validation, Project administration, Funding acquisition. **R. Velraj:** Conceptualization, Methodology, Writing - review & editing, Supervision. **I. Lynch:** Data curation, Writing - review & editing, Validation. Navid Aslfattahi**:** Writing - review & editing.

Declaration of Competing Interest

The authors declare that they have no known competing financial interests or personal relationships that could have appeared to influence the work reported in this paper.

Nomenclature

A_g	:	Area of SS glass cover (m^2)
$h_{c,ab-w}$	:	Convective heat transfer coefficient between absorber and water (W/m^2 K)
$h_{c,w-g}$	:	Convective heat transfer coefficient between water and glass (W/m^2 K)
$h_{e,w-g}$	:	Evaporative heat transfer coefficient between water and glass (W/m^2 K)
I_t	:	Solar radiation (W/m^2)
L_{fg}	:	Latent heat of evaporation (J/kg)
m_w	:	Water yield (kg)
P_g	:	Partial vapor pressure at glass surface (N/m^2)
P_w	:	Partial vapor pressure at water surface (N/m^2)
$Q_{c,ab-w}$	:	Convective heat transfer rate between absorber and water (W)
T_{ab}	:	Absorber plate temperature (°C)
T_{amb}	:	Ambient temperature (°C)
T_g	:	Glass cover temperature (°C)

T_w	:	Water temperature (°C)
U_b	:	Bottom heat loss coefficient between water and atmosphere (W/m^2K)

Greek symbol

α_{ab}	:	Absorptivity of absorber
η_{ene}	:	Average energy efficiency
τ_g	:	Solar transmittance of glass
τ_w	:	Solar transmittance of water
Δt	:	Time difference (s)

Abbreviation

CSS	:	Conventional solar still
R	:	Thermal resistance
SS	:	Solar still
TC	:	Thermal conductivity
TGA	:	Thermo gravimetric analysis
UV-Vis	:	Ultraviolet-visible spectrometry
XRD	:	X-ray diffraction

References

1. R. Sathyamurthy, S.A. El-Agouz, V. Dharmaraj, Experimental analysis of a portable solar still with evaporation and condensation chambers, Desalination 367 (2015) 180-185,
2. S.A. Kalogirou, Seawater desalination using renewable energy sources, Prog. Energy Combust. Sci. 31 (2005) 242-281.
3. S. Gorjian, B. Ghobadian, T.T. Hashjin, A. Banakar, Experimental performance evaluation of a stand-alone point-focus parabolic solar still, Desalination 352 (2014) 1-17.

4. M. Elimelech , W.A. Phillip , The future of seawater desalination: energy, technology, and the environment, Science 333 (6043) (2011) 712–717.
5. Fritzmann C, Löwenberg J, Wintgens T, Melin T. State-of-the-art of reverse osmosis desalination. Desalination 2007;216(1–3):1–76.
6. Khawaji AD, Kutubkhanah IK, Wie J-M. Advances in seawater desalination technologies. Desalination 2008;221(1–3):47–69.
7. Al-Hallaj S, Farid MM, Tamimi AR. Solar desalination with a humidification dehumidification cycle: performance of the unit. Desalination 1998; 120 (3):273–80.
8. Viala E. Water for food, water for life a comprehensive assessment of water management in agriculture. Springer; 2008.
9. Fath HE. Solar distillation: a promising alternative for water provision with free energy, simple technology and a clean environment. Desalination 1998;116(1):45–56
10. W.M. Alaian , E.A. Elnegiry , A.M. Hamed , Experimental investigation on the performance of solar still augmented with pin-finned wick, Desalination 379 (2016) 10–15.
11. A. Shyora , K. Patel , H. Panchal , Comparative analysis of stepped and single basin solar still in climate conditions of Gandhinagar Gujarat during winter, Int. J. Ambient Energy (2019) 1–11 .
12. Elmaadawy, Khaled, A. W. Kandeal, Ahmed Khalil, M. R. Elkadeem, Bingchuan Liu, and Swellam W. Sharshir. Performance improvement of double slope solar still via combinations of low cost materials integrated with glass cooling. Desalination 500 (2021): 114856.
13. A.K. Thakur, R. Sathyamurthy, W.S. Sharshir, A.E. Kabeel, Ma Z. Elkadeem, A. M. Manokar, M. Arıcı, A.K. Pandey, R. Saidur, Performance analysis of a modified solar still

using reduced graphene oxide coated absorber plate with activated carbon pellet, Sustain. Energy Technol. Assess. 45 (2021) 101046.

14. A.K. Thakur, R. Sathyamurthy, R. Velraj, I. Lynch, R. Saidur, A.K. Pandey, W.S. Sharshir, Z. Ma, P. GaneshKumar, A.E. Kabeel. Sea-water desalination using a desalting unit integrated with a parabolic trough collector and activated carbon pellets as energy storage medium. Desalination 516 (2021) 115217.
15. S.W. Sharshir, A.H. Elsheikh, Y.M. Ellakany, A.W. Kandeal, E.M.A. Edreis, R. Sathyamurthy, A.K. Thakur, M.A. Eltawil, M.H. Hamed, Improving the performance of solar still using different heat localization materials, Environ. Sci. Pollut. Res. 27 (11) (2020) 12332–12344.
16. A.K. Thakur, P. Khandelwal, B. Sharma, Productivity comparison of solar still with nano fluid and phase changing material with same depth of water, in: G. Anand, J. Pandey, S. Rana (Eds.), Nanotechnology for Energy and Water. ICNEW 2017. Proceedings in Energy, Springer, Cham, 2018.
17. A.K. Thakur, R. Sathyamurthy, R. Velraj, R. Saidur, J.Y. Hwang, Augmented performance of solar desalination unit by utilization of nano-silicon coated glass cover for promoting drop-wise condensation, Desalination 515 (2021), 115191.
18. A.K. Thakur, S.W. Sharshir, Z. Ma, A. Thirugnanasambantham, S.S. Christopher, M. P. Vikram, S. Li, P. Wang, W. Zhao, A.E. Kabeel, Performance amelioration of single basin solar still integrated with V-type concentrator: energy, exergy, and economic analysis, Environ. Sci. Pollut. Res. 28 (2021) 3406–3420.
19. Arunkumar, T., Murugesan, D., Viswanathan, C. et 564 al. Effect of CuO, MoO3 and ZnO nanomaterial coated absorbers for clean water production. SN Appl. Sci. 2, 1709 (2020).

20. Thakur AK, Sathyamurthy R, Sharshir WS, Ahmed MS, Hwang JY (2020) A novel reduced graphene oxide based absorber for augmenting the water yield and thermal performance of solar desalination unit. Mater Lett 286:128867.
21. Sathyamurthy R, Kabeel AE, Balasubramanian M, Devarajan M, Sharshir SW, Manokar AM (2020) Experimental study on enhancing the yield from stepped solar still coated using fumed silica nanoparticle in black paint. Mater Lett 272:127873.
22. Kabeel AE, Sathyamurthy R, Sharshir SW, Muthumanokar A, Panchal H, Prakash N, Prasad C,Nandakumar S, El KadyMS (2019) Effect of water depth on a novel absorber plate of pyramid solar still coated with TiO_2 nano black paint. J Clean Prod 213:185–191
23. Karthik, K. V., A. V. Raghu, Kakarla Raghava Reddy, R. Ravishankar, M. Sangeeta, Nagaraj P. Shetti, and Ch Venkata Reddy. "Green synthesis of Cu-doped ZnO nanoparticles and its application for the photocatalytic degradation of hazardous organic pollutants." Chemosphere 287 (2022): 132081.
24. Kannan, Karthik, D. Radhika, Kakarla Raghava Reddy, Anjanapura V. Raghu, Kishor Kumar Sadasivuni, Geetha Palani, and K. Gurushankar. "Gd3+ and Y3+ co-doped mixed metal oxide nanohybrids for photocatalytic and antibacterial applications." Nano Express 2, no. 1 (2021): 010014.
25. Jonnalagadda, Madhavi, Vishnu Bhotla Prasad, and Anjanapura V. Raghu. "Synthesis of composite nanopowder through Mn doped ZnS-CdS systems and its structural, optical properties." Journal of Molecular Structure 1230 (2021): 129875.
26. Shwetharani, R., H. R. Chandan, M. Sakar, Geetha R. Balakrishna, Kakarla Raghava Reddy, and Anjanapura V. Raghu. "Photocatalytic semiconductor thin films for hydrogen production

and environmental applications." International Journal of Hydrogen Energy 45, no. 36 (2020): 18289-18308.

27. Madhavi, Jonnalagadda, V. Prasad, Kakarla Raghava Reddy, Ch Venkata Reddy, and Anjanapura V. Raghu. "Facile synthesis of Ni-doped ZnS-CdS composite and their magnetic and photoluminescence properties." Journal of Environmental Chemical Engineering 9, no. 6 (2021): 106335.
28. A.K. Thakur, J.Y. Hwang, R. Sathyamurthy. A State of Art Critical Review on Advancement in MXenes for Electrochemical Energy Storage in the View of Interlayer Spacing. ECS Trans. 99 (2020) 143.
29. Abdelrazik A.S., Tan K.H., Aslfattahi N., Arifutzzaman A., Saidur R., Al-Sulaiman F.A. Optical, stability and energy performance of water-based MXene nanofluids in hybrid PV/thermal solar systems. Solar Energy 204 (2020) 32-47.
30. L. Ding, Y. Wei, L. Li, T. Zhang, H. Wang, J. Xue, L.X. Ding, S. Wang, J. Caro, Y. Gogotsi, MXene molecular sieving membranes for highly efficient gas separation, Nat Commun, 9 (2018) 155.
31. F. Shahzad, M. Alhabeb, C.B. Hatter, B. Anasori, H.S. Man, C.M. Koo, Y. Gogotsi, Electromagnetic interference shielding with 2D transition metal carbides (MXenes), Science, 353 (2016) 1137-1140.
32. A. Lipatov, H. Lu, M. Alhabeb, B. Anasori, A. Gruverman, Y. Gogotsi, A. Sinitskii, Elastic properties of 2D Ti3C2T x MXene monolayers and bilayers, Science Advances, 4 (2018) eaat0491.

33. Y. Xia, T.S. Mathis, M.Q. Zhao, B. Anasori, A. Dang, Z. Zhou, H. Cho, Y. Gogotsi, S. Yang, Thickness-independent capacitance of vertically aligned liquid-crystalline MXenes, Nature, 557 (2018) 409-412.

34. K. Li, T.H. Chang, Z. Li, H. Yang, F. Fu, T. Li, J.S. Ho, P.Y. Chen, Biomimetic MXene Textures with Enhanced Light-to-Heat Conversion for Solar Steam Generation and Wearable Thermal Management, Advanced Energy Materials, 9 (2019) 1901687.

35. T. Liu, X. Liu, N. Graham, W. Yu, K. Sun, Two-dimensional MXene incorporated graphene oxide composite membrane with enhanced water purification performance, Journal of Membrane Science, 593 (2020) 117431.

36. X. Xie, C. Chen, N. Zhang, Z.-R. Tang, J. Jiang, Y.-J. Xu, Microstructure and surface control of MXene films for water purification, Nature Sustainability, 2 (2019) 856-862.

37. X. Ming, A. Guo, Q. Zhang, Z. Guo, F. Yu, B. Hou, Y. Wang, K.P. Homewood,X. Wang, 3D macroscopic graphene Oxide/MXene architectures for multifunctional water purification, Carbon (2020).

38. Li, R., Zhang, L., Shi, L., Wang, P. MXene Ti3C2: An Effective 2D Light-to-Heat Conversion Material. ACS Nano 2017, 11, 4, 3752–3759.

39. Li, K. R., Chang, T.-H., Li, Z. P., Yang, H. T., Fu, F. F., Li, T. T., Ho, J. S., Chen, P.-Y., Biomimetic MXene Textures with Enhanced Light-to-Heat Conversion for Solar Steam Generation and Wearable Thermal Management. Adv. Energy Mater. 2019, 9, 1901687.

40. Das, L.; Habib, K.; Saidur, R.; Aslfattahi, N.; Yahya, S.M.; Rubbi, F. Improved Thermophysical Properties and Energy Efficiency of Aqueous Ionic Liquid/MXene Nanofluid in a Hybrid PV/T Solar System. Nanomaterials 2020, 10, 1372.

41. H E S Fatha, M El-Samanoudy, K Fahmy, A Hassabou, Thermal-economic analysis and comparison between pyramid-shaped and single-slope solar still configurations, Desalination 159 (2003) 69–79.
42. El-Sebaii AA, Al-Ghamdi AA, Al-Hazmi FS, Faidah AS. Thermal performance of a single basin solar still with PCM as a storage medium. Appl Energy. 2009;86(7–8):1187–95.
43. Dhivagar, R., Mohanraj, M., Hidouri, K. et al. Energy, exergy, economic and enviro-economic (4E) analysis of gravel coarse aggregate sensible heat storage-assisted single-slope solar still. J Therm Anal Calorim 145, 475–494 (2021).
44. Alaa H. Salah, Gasser E. Hassan, Hassan Fath, Mohamed Elhelw, Samy Elsherbiny, Analytical investigation of different operational scenarios of a novel greenhouse combined with solar stills, Appl. Thermal Eng. 122 (2017) 297–310.
45. M. Ghidiu, et al., Conductive two-dimensional titanium carbide ‘clay'with high volumetric capacitance, Nature 516 (7529) (2014) 78.
46. Li Z, Wang L, Sun D, Zhang Y, Liu B, Hu Q, et al. Synthesis and thermal stability of two-dimensional carbide MXene Ti3C2. Mater Sci Eng, B 2015; 191:33–40.
47. Arani RP, Sathyamurthy R, Chamkha A, Kabeel AE, Deverajan M, Kamalakannan K, Balasubramanian M, Manokar AM, Essa F, Saravanan A. Effect of fins and silicon dioxide nanoparticle black paint on the absorber plate for augmenting yield from tubular solar still. Environ Sci Pollut Res Int. 2021 Jul;28(26):35102-35112.
48. Liu R., Li W. High-thermal-stability and high-thermal-conductivity Ti3C2Tx MXene/Poly (vinyl alcohol) (PVA) composites. ACS Omega. 2018; 3:2609–2617.
49. Chen L, Shi X, Yu N, Zhang X, Du X, Lin J. Measurement and Analysis of Thermal Conductivity of Ti_3C_2Tx MXene Films. Materials (Basel). 2018;11(9):1701.

50. Ling Z., Ren C.E., Zhao M.Q., Yang J., Giammarco J.M., Qiu J.S., Barsoum M.W., Gogotsi Y. Flexible and conductive MXene films and nanocomposites with high capacitance. Proc. Natl. Acad. Sci. USA. 2014;111:16676–16681.
51. S.W. Sharshir , G. Peng , A.H. Elsheikh , E.M.A. Edreis , M.A. Eltawil , T. Abdel- hamid , A.E. Kabeel , J. Zang , N. Yang , Energy and exergy analysis of solar stills with micro/nano particles: a comparative study, Energy Convers. Manage. 177 (2018) 363–375.
52. Wang, H, Li, X, Luo, B, Wei, K, Zeng, G. The MXene/water nanofluids with high stability and photo-thermal conversion for direct absorption solar collectors: A comparative study. Energy 227 (2021) 120483.
53. Wiscombe WJ. Improved Mie scattering algorithms. Appl Opt 1980;19(9):1505-9.
54. Total dissolved solids in Drinking-water, World Health Organization 2003. Available: http://www.who.int/water_sanitation_health/dwq/chemicals/tds.pdf
55. pH in Drinking-water, World Health Organization 2007. Available: http://www.who.int/water_sanitation_health/dwq/chemicals/ph_revised_2007_clean_version.pdf
56. Water quality standards, WHO 2011, http://mrccc.org.au/wp-content/uploads/2013/10/Water-Quality-Salinity-Standards.pdf